

Global Biogeochemical Cycles®

RESEARCH ARTICLE

10.1029/2023GB007921

Transport of Anthropogenic Carbon From the Antarctic Shelf to Deep Southern Ocean Triggers Acidification

Key Points:

- We show evidence for the accumulation of C_{ant} along the Antarctic shelf-slope into the deep ocean
- The process of AABW formation drives C_{ant} downward transport at $25.0 \pm 4.7 \text{ Tg C yr}^{-1}$, sustaining the CO_2 uptake in the surface ocean
- This further triggers acidification of AABW at a rate of $-0.0006 \pm 0.0001 \text{ pH unit yr}^{-1}$, which is faster than in other deep oceans

Supporting Information:

Supporting Information may be found in the online version of this article.

Correspondence to:

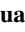





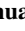

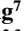

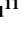
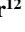

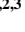

D. Qi, Y. Wu and L. Chen,
qidi@jmu.edu.cn;
yingxu.wu@jmu.edu.cn;
chenliqi@jmu.edu.cn

Citation:

Zhang, S., Wu, Y., Cai, W.-J., Cai, W., Feely, R. A., Wang, Z., et al. (2023). Transport of anthropogenic carbon from the Antarctic shelf to deep Southern Ocean triggers acidification. *Global Biogeochemical Cycles*, 37, e2023GB007921. <https://doi.org/10.1029/2023GB007921>

Received 24 JUL 2023
 Accepted 18 NOV 2023
 Corrected 31 DEC 2023

This article was corrected on 31 DEC 2023. See the end of the full text for details.

Shuang Zhang^{1,2,3} , Yingxu Wu² , Wei-Jun Cai⁴ , Wenju Cai⁵ , Richard A. Feely⁶ , Zhaomin Wang⁷ , Toste Tanhua⁸ , Yanmin Wang^{2,3}, Chengyan Liu⁷, Xichen Li⁹ , Qinghua Yang⁷ , Minghu Ding¹⁰ , Zhongsheng Xu¹¹ , Rodrigo Kerr¹² , Yiming Luo⁷ , Xiao Cheng⁷, Liqi Chen^{1,2,3} , and Di Qi^{2,7} 

¹State Key Lab of Marine Environmental Science, Xiamen University, Xiamen, China, ²Polar and Marine Research Institute, Jimei University, Xiamen, China, ³The Third Institute of Oceanography (TIO), MNR, Xiamen, China, ⁴School of Marine Science and Policy, University of Delaware, Newark, DE, USA, ⁵Centre for Southern Hemisphere Oceans Research (CSHOR), CSIRO Oceans and Atmosphere, Hobart, TAS, Australia, ⁶Pacific Marine Environmental Laboratory, National Oceanic and Atmospheric Administration, Seattle, WA, USA, ⁷Southern Marine Science and Engineering Guangdong Laboratory (Zhuhai), Zhuhai, China, ⁸GEOMAR Helmholtz Centre for Ocean Research Kiel, Kiel, Germany, ⁹International Center for Climate and Environment Sciences, Institute of Atmospheric Physics, Chinese Academy of Sciences, Beijing, China, ¹⁰Chinese Academy of Meteorological Sciences, Beijing, China, ¹¹Key Laboratory of Marine Ecosystem and Biogeochemistry, Second Institute of Oceanography, Ministry of Natural Resources (MNR), Hangzhou, China, ¹²Laboratório de Estudos dos Oceanos e Clima, Instituto de Oceanografia, Universidade Federal do Rio Grande (FURG), Rio Grande, Brazil

Abstract Flow of dense shelf water provide an efficient mechanism for pumping CO_2 to the deep ocean along the continental shelf slope, particularly around the Antarctic bottom water (AABW) formation areas where much of the global bottom water is formed. However, the contribution of the formation of AABW to sequestering anthropogenic carbon (C_{ant}) and its consequences remain unclear. Here, we show prominent transport of C_{ant} ($25.0 \pm 4.7 \text{ Tg C yr}^{-1}$) into the deep ocean ($>2,000 \text{ m}$) in four AABW formation regions around Antarctica based on an integrated observational data set (1974–2018). This maintains a lower C_{ant} in the upper waters than that of other open oceans to sustain a stronger CO_2 uptake capacity ($16.9 \pm 3.8 \text{ Tg C yr}^{-1}$). Nevertheless, the accumulation of C_{ant} can further trigger acidification of AABW at a rate of $-0.0006 \pm 0.0001 \text{ pH unit yr}^{-1}$. Our findings elucidate the prominent role of AABW in controlling the Southern Ocean carbon uptake and storage to mitigate climate change, whereas its side effects (e.g., acidification) could also spread to other ocean basins via the global ocean conveyor belt.

Plain Language Summary The Southern Ocean is thought to uptake and store a large amount of anthropogenic CO_2 (C_{ant}), but little attention has been paid to the Antarctic coastal regions in the south of 60°S , mainly due to the lack of observations. Based on an integrated data set, we discovered the deep penetration of C_{ant} and a visible pattern of relatively high concentration of C_{ant} along the AABW formation pathway, and the concentration of C_{ant} along the shelf-slope is higher than that of other marginal seas at low-mid latitudes, implying a highly effective C_{ant} transport in AABW formation areas. We also found strong upper-layer CO_2 uptake and a significant acidification rate in the deep waters of the Southern Ocean due to the AABW-driven CO_2 transport, which is 3 times faster than those in other deep oceans. It is therefore crucial to understand how the Antarctic shelf regions affect the global carbon cycle through the uptake and transport of anthropogenic CO_2 , which also drives acidification in the other ocean basins.

1. Introduction

The Southern Ocean (SO) plays a critical role in ventilating the global oceans and regulating the earth's climate through the uptake and storage of atmospheric CO_2 on centennial-millennium timescale (Rae et al., 2018), being responsible for $\sim 40\%$ of the global oceanic uptake of anthropogenic CO_2 (C_{ant}) (Gruber et al., 2019; Khatiwala et al., 2009). The ongoing absorption of C_{ant} is ensured by the unique ocean circulation in this region, where C_{ant} is mainly transported and subducted by the Antarctic Intermediate Water (AAIW), Sub-Antarctic Mode Water (SAMW), and Antarctic bottom water (AABW) (Ito et al., 2010). Major efforts to assess the carbon balance of the Southern Ocean have focused on quantifying the air-sea CO_2 flux and the C_{ant} inventory in the upper cell of the Meridional Overturning Circulation (Bopp et al., 2015; DeVries et al., 2017; Ito et al., 2010; Sallée et al., 2012),

whereas less is paid on the Antarctic coastal regions affected by the lower cell of overturning circulation because previous studies based on carbon inventory suggested that these regions are characterized by a negligible carbon sink due to the influence of upwelling of CO₂-rich deep waters and seasonal sea-ice formation that physically blocked the air-sea CO₂ exchange (Gruber et al., 2019; Poisson & Chen, 1987; Sabine et al., 2004).

Some evidence to the contrary showed that the upwelling of Circumpolar Deep Water (CDW), characterized by depleted C_{ant} , is preferential for the uptake of anthropogenic CO₂ (DeVries, 2014; DeVries et al., 2017), and sea-ice blockage could enhance CO₂ uptake by suppressing winter CO₂ outgassing (Du et al., 2022; Shadwick et al., 2021). Modeling studies demonstrated that C_{ant} inventories in the ocean interior were not always appropriate for assessing the local carbon uptake capacity, as the apparent asymmetry between them was attributed to the rapid northward transport of C_{ant} into the sub-Antarctic zone (DeVries, 2014; Sarmiento et al., 1992). The ability of the Antarctic deep-water formation regions to regulate the air-sea CO₂ balance and to act as a carbon sink was partially confirmed (Arrigo et al., 2008; Bourgeois et al., 2016; Marinov et al., 2006; Nissen et al., 2022). However, ocean models are difficult to correctly simulate all the processes involved in AABW formation above the continental shelves (de Lavergne et al., 2014; Heuzé, 2021), which is associated with sea-ice formation, surface cooling, and mixing with ambient water as it cascades down the continental slope (Foster & Carmack, 1976). A few recent studies (Gao et al., 2022; Mahieu et al., 2020; Ríos et al., 2012) imply that AABW has a high C_{ant} concentration and might even influence the C_{ant} of adjacent deep oceans (e.g., South Atlantic) by advection. Therefore, the contribution of the AABW formation to the transport of C_{ant} from the Antarctic shelf into the deep Southern Ocean and the consequences of this transport need to be clarified.

Here we use data from a combination of the Global Ocean Data Analysis Project (Lauvset et al., 2022) version 2022 (GLODAPv2.2022) and the Chinese Antarctic Research Expedition (CHINARE) to report the distribution of C_{ant} in the Antarctic coastal regions (particularly the AABW formation regions Weddell Sea, Ross Sea, Prydz Bay, and Adélie Land) based on three different approaches. The phenomenon is presented in a climatological way (average over a period 1974–2018) by integrating all the available data. We propose an AABW-formation-driven mechanism to explain the prominent downward transport of C_{ant} and its link with CO₂ uptake in the surface ocean. We further diagnose and evaluate the consequences of carbon export to and accumulation in the abyssal Southern Ocean, which leads to long-term acidification in the deep waters.

2. Methods

2.1. Study Area and Data

Antarctic shelves are typically categorized into non-cold and cold depending on the relative environmental conditions and their efficiency for deep transport (Petty et al., 2013). The non-cold shelf region is flooded by warm Circumpolar Deep Water (CDW) and is unfavorable for bottom water formation (Lee et al., 2017), whereas the cold shelf region is characterized by cooler seafloor temperatures and is therefore conducive to bottom water formation, including four major AABW formation sites (Solodoch et al., 2022).

Water samples throughout the water column were collected using Niskin bottles along six transects from Prydz Bay aboard the R/V XueLong during the 31st Chinese National Antarctic Research Expedition (CHINARE 31, Figure S1a in Supporting Information S1; Liu et al., 2023) from 05 February to 02 March 2015. Hydrographic data were measured with an SBE-911plus conductivity-temperature-depth (CTD) unit (Sea-Bird, USA), which measured practical salinity (± 0.002), temperature ($\pm 0.001^\circ\text{C}$), and pressure (0.015% of full scale). Measurements and quality control of carbonate chemistry parameters are described in Text S1 and Figure S2 in Supporting Information S1 and follow the “Guide to Best Practices for Ocean CO₂ Measurements” (Dickson et al., 2007) with respect to marine carbonate systems.

Other DIC and TA data in the four Antarctic cold shelves in Figure S1b of the Supporting Information S1 were downloaded from the GLODAPv2.2022 data set (Lauvset et al., 2022). Cruises are listed in Table S1 of the Supporting Information S1 and the synthetic data set shown in Figure S1 of the Supporting Information S1 was used in this study.

In situ pH and other related parameters were calculated from DIC, TA, temperature, salinity and nutrients (phosphate and silicate) using the Matlab version of CO2SYS v1.1 (S. Van Heuven et al., 2011). In order to make full use of DIC and TA data (because some of them are not accompanied with phosphate and silicate concentrations),

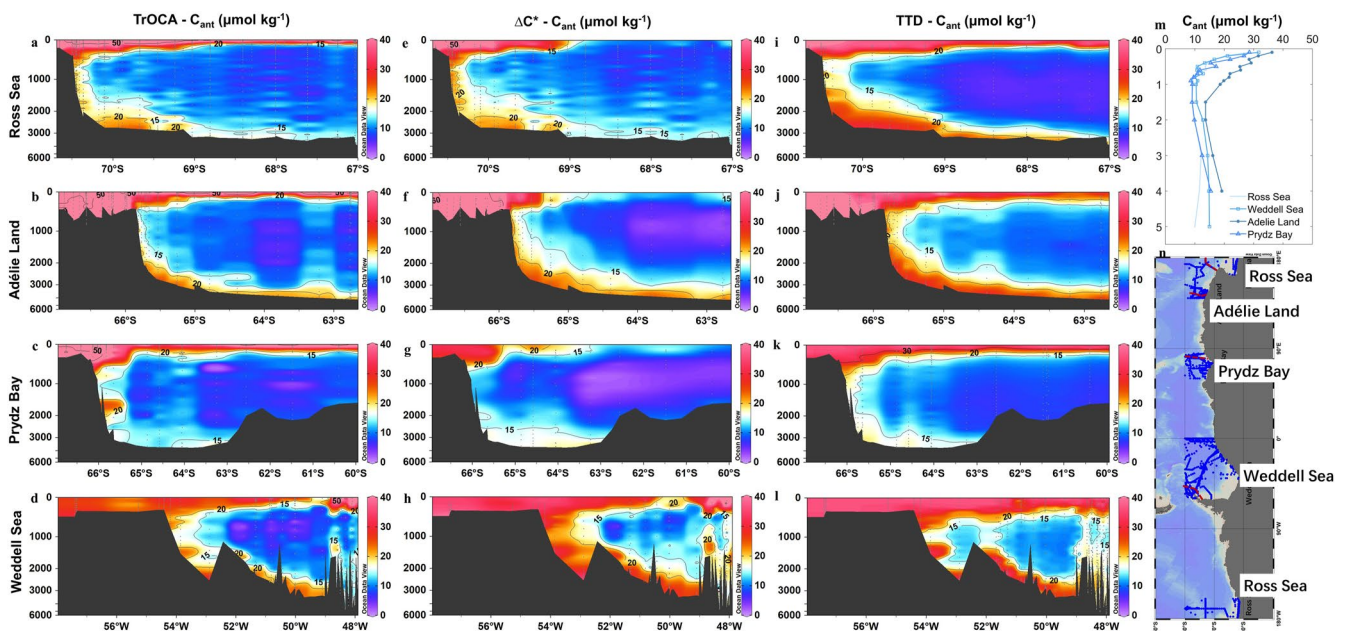


Figure 1. Vertical distributions of C_{ant} in Adélie Land, Weddell Sea, Ross Sea, and Prydz Bay using the TrOCA, ΔC^* , and TTD approaches. Four cold shelves are defined as Adélie Land (60° – 90° S, 140° – 150° E), Weddell Sea (60° – 90° S, 0° – 60° W), Ross Sea (60° – 90° S, 150° – 180° E, 160° – 180° W) and Prydz Bay (60° – 90° S, 60° – 85° E). The red solid lines in (n) indicate the sections in (a)–(l). The vertical distribution of TrOCA-based C_{ant} in four cold shelves is shown in (m). Water masses are defined by the neutral density (γ_n) in (e), combined with depth, temperature, and salinity in Table S3 of the Supporting Information S1. The Weddell Sea and Ross Sea have wide continental shelves, the Prydz Bay and Adélie Land have the narrow continental shelves in (n). Figures were made with Ocean Data View version 5.6.2 (Schlitzer, 2023).

we used the mean values of phosphate and silicate concentrations (from GLODAPv2.2022 and CHINARE31 data sets) for the missing nutrient values in AABW in each region. Carbonate dissociation constants were taken from Lueker et al. (2000), K_{sp} from Mucci (1983), K_{so4} from Dickson (1990) and total boron from Lee et al. (2010).

2.2. Anthropogenic CO_2 Calculation

Based on the integrated data (Figure S1 in Supporting Information S1), we estimated and compared C_{ant} throughout the water column using three different approaches; the TrOCA approach, the ΔC^* approach and the TTD approach (Gruber et al., 1996; Touratier & Goyet, 2004a; Waugh et al., 2006). We also evaluated air-sea fluxes in the Antarctic coastal seas (Text S2 in Supporting Information S1).

2.2.1. TrOCA Approach

The TrOCA (Tracer combining O_2 , TCO_2 , TA) method was originally proposed by Touratier (Touratier & Goyet, 2004a, 2004b) to calculate anthropogenic CO_2 concentrations. The conservative tracer TrOCA was defined as in Equation 1 (Touratier et al., 2007). The pre-industrial TrOCA and $TrOCA^0$ values derived from $\Delta^{14}C$ and CFC-11 were combined and fitted with the following exponential function (Equation 2 based on the GLODAP world ocean database (<http://cdiac.ornl.gov/oceans/glodap/Glodaphome.htm>)). The anthropogenic CO_2 concentration (C_{ant_TrOCA}) in Figures 1a–1d was then estimated using Equation 3. This has been applied previously in the Antarctic regions (Sandrini et al., 2007; Shadwick et al., 2014; S. M. A. C. van Heuven et al., 2011). It is noteworthy that the TrOCA method, as well as the other back calculation methods, remains subject to large uncertainties when it was applied in the upper mixed layer (e.g., 150 m; Gruber et al., 2019), where biological processes and air-sea CO_2 fluxes modify the carbon content of the upper ocean on a short time scale.

$$TrOCA = O_2 + a \left(DIC - \frac{1}{2} TA \right) \quad (1)$$

$$TrOCA^0 = e^{\left(7.511 - (1.087 \times 10^{-2}) \theta - \frac{7.81 \times 10^5}{TA^2} \right)} \quad (2)$$

$$C_{\text{ant_TrOCA}} = \frac{\text{TrOCA} - \text{TrOCA}^0}{a} = \frac{O_2 + 1.279 \left(\text{DIC} - \frac{1}{2} \text{TA} \right) - e^{\left(\frac{7.511 - (1.087 \times 10^{-2}) \theta - \frac{7.81 \times 10^5}{\text{TA}^2} \right)}}{1.279} \quad (3)$$

where θ is potential temperature, °C; O_2 is dissolved oxygen, $\mu\text{mol kg}^{-1}$; DIC is total inorganic carbon, $\mu\text{mol kg}^{-1}$; TA is total alkalinity, $\mu\text{mol kg}^{-1}$; $C_{\text{ant_TrOCA}}$ is anthropogenic CO_2 concentration estimated from TrOCA, $\mu\text{mol kg}^{-1}$.

2.2.2. ΔC^* Approach

The quasi-conservative tracer, ΔC^* , was defined as the difference between the measured DIC (C_m) and the pre-industrial preformed DIC in equilibrium with the atmosphere (C_{280}) in Equation 4. The biological term (ΔC_{bio}) included organic remineralization, dissolution of calcium carbonate particles and denitrification. The organic component could be estimated from the changes in AOU together with the stoichiometric ratios ($C/O_2 = 117/170$, $N/O_2 = 16/170$) (Anderson & Sarmiento, 1994). The oxygen utilization should be corrected on the basis of the Optimum Multiparameter (OMP) analysis (Text S3 in Supporting Information S1) due to the real unsaturated state of oxygen in polar regions (Lo Monaco, Goyet, et al., 2005; Lo Monaco, Metzl, et al., 2005). The latter components could be obtained from the difference between the measured TA and a preformed TA (TA^0) and a denitrification correction to the biological with a denitrification ratio of 106/104 (Gruber & Sarmiento, 1997), as in Equation 5. The TA^0 values (Equation 6) were based on a multiple linear regression fit of surface TA values from different cruises in the Pan-Antarctic region (around the Antarctic seas; Figure S3 in Supporting Information S1). The air-sea disequilibrium component (ΔC_{diseq}) could be distinguished from the anthropogenic signal using either water age information (from CFC-12) or the distribution of ΔC^* in regions that was not affected by the anthropogenic transient (Sabine et al., 2004) (as in Equation 7). For given isopycnal surfaces, we assumed that the C_{ant} was zero over some portion of an isopycnal surface, the ΔC_{diseq} was set equal to the average of the ΔC^* values for that portion of the surface (Sabine et al., 2004). We used an OMP analysis to evaluate the relative contributions of the different water sources (Figure S4 in Supporting Information S1) on individual isopycnal surfaces to obtain the net air-sea disequilibrium values (Table S2 in Supporting Information S1). This method has been applied to the global oceans (Gruber, 1998; Sabine et al., 2002, 2004).

$$\Delta C^* = C_m - \Delta C_{\text{bio}} - C_{280} \quad (4)$$

$$\Delta C^* = C_m - C_{280} + 117/170(O - O_{\text{sat}}) - 1/2(\text{TA} - \text{TA}^0 - 16/170(O - O_{\text{sat}})) + 106/104 N_{\text{anom}}^* \quad (5)$$

$$\text{TA}^0 = 20.2208 + 69.1934 * S - 0.1123 * \text{PO} - 2.9645 * \theta \quad (6)$$

$$C_{\text{ant_star}} = C_m - \Delta C_{\text{bio}} - C_{280} - \Delta C_{\text{diseq}} = \Delta C^* - \Delta C_{\text{diseq}} \quad (7)$$

where $C_{\text{ant_star}}$ denotes to anthropogenic carbon concentration, C_m denotes to measured DIC concentration in $\mu\text{mol kg}^{-1}$, ΔC_{bio} denotes to DIC ($\mu\text{mol kg}^{-1}$) changes due to remineralization of organic matter and dissolution of calcium carbonate particles, C_{280} denotes to DIC ($\mu\text{mol kg}^{-1}$) of waters in equilibrium with an atmospheric CO_2 concentration of 280 μatm , PO is a quasi-conservative tracer introduced by Broecker (1974). N_{anom}^* is the N^* anomaly from the mean as the denitrification correction.

2.2.3. Transit Time Distribution (TTD) Approach

The application of the TTD method to C_{ant} concentration estimation was described by Waugh et al. (2004). It was based on several assumptions: (a) the circulation was in a steady-state, (b) a single surface source region dominated the C_{ant} at each interior location, (c) the TTD of the ocean could be approximated by a 1-D advection-diffusion equation, known as the “inverse Gaussian,” and (d) the disequilibrium of carbon between the atmosphere and the surface ocean was constant with time (Waugh et al., 2004, 2006). $C_{\text{ant},t}$ at any point in the interior of the ocean, was related to the history of surface C_{ant} and the range of times it took to reach its sequestration location (Equations 8 and 9). Thus, assuming that C_{ant} behaves as an inert passive tracer (Waugh et al., 2006), C_{ant} could be estimated using the IG-TTD model (Equation 10) (Waugh et al., 2004).

$$c(r, t) = \int_0^{\infty} c_0(t - t') G(r, t') dt' \quad (8)$$

Table 1

C_{ant} Concentrations in the Main Antarctic Water Masses and Fluxes (Net C_{ant} Export Fluxes Through Air-Sea Exchange in Four Cold Shelves and the Pan-Antarctica)

Areas	Ventilation rates DSW ^a (Sv)	C _{ant} in DSW ΔC ^a (TTD) ^b (μmol kg ⁻¹)	C _{ant} in mCDW ΔC ^a (TTD) ^b (μmol kg ⁻¹)	C _{ant} in AABW ΔC ^a (TTD) ^b (μmol kg ⁻¹)	C _{ant} in AABW TrOCA ^b (μmol kg ⁻¹)	Gross flux TrOCA ^c (Tg C yr ⁻¹)	Net export flux TrOCA ^c (Tg C yr ⁻¹)	CO ₂ uptake ^d (Tg C yr ⁻¹)
Prydz Bay	0.52 ± 0.26	38 ± 20 (34 ± 1)	22 ± 8	14 ± 4	14 ± 4	6.46 ± 3.21	2.06 ± 1.01	-2.31 ± 1.39
Weddell Sea	3.40 ± 0.60	35 ± 2 (33 ± 1)	14 ± 10	18 ± 10 (16 ± 7)	14 ± 4	35.58 ± 6.42	17.16 ± 3.03	-3.74 ± 2.75
Ross Sea	0.98 ± 0.93	37 ± 6 (33 ± 2)	19 ± 6	21 ± 7 (24 ± 5)	15 ± 5	10.46 ± 8.61	3.20 ± 2.76	-9.12 ± 2.13
Adélie Land	0.30 ± 0.28	51 ± 4 (36 ± 1)	23 ± 9	24 ± 10 (25 ± 6)	18 ± 5	5.17 ± 4.39	2.57 ± 2.07	-2.02 ± 0.85
Four cold shelf ^e	5.20 ± 0.32	40 ± 8 (34 ± 1)	20 ± 8	21 ± 8 (22 ± 6)	15 ± 4	57.7 ± 12.0	25.0 ± 4.7	-16.9 ± 3.8
Pan-Antarctica ^f	5.40 ± 1.70	40 ± 8 (34 ± 1)	20 ± 8	21 ± 8 (22 ± 6)	15 ± 4	68.6 ± 12.8	28.1 ± 6.2	-30.9 ± 6.1

^aDSW ventilation rates in Section 2. ^bMean C_{ant} concentrations in DSW, mCDW, and AABW by TrOCA, ΔC* and TTD methods were derived from the average of all C_{ant} values from 1974 to 2018 based on the GLODAPv2.2022 data set (see “Anthropogenic CO₂ calculation—TrOCA approach, ΔC* approach and TTD” in Section 2). ^cThe range of export fluxes was estimated from the mean of all annual C_{ant} values based on the TrOCA method according to Equations 11 and 12 in Section 2. ^dThe CO₂ uptake flux is filtered by latitude (>60°S) in Table S5 of the Supporting Information S1. A negative value indicates that the ocean is absorbing CO₂ from the atmosphere. ^eThe ventilation rate of the four cold shelves was calculated from the sum of the rates of the four cold shelves above. The total of the C_{ant} values were the average data from Adélie Land, Weddell Sea, Ross Sea and Prydz Bay. The net export flux was based on the mean of C_{ant} concentrations in four cold shelves and their total ventilation rates (total areas) of them. The CO₂ uptake flux of four cold shelves was based on the sum of CO₂ uptake flux in four cold shelves above. ^fThe ventilation rate of the Pan-Antarctic includes all sites and regions that could produce AABW around Antarctica, including four cold shelves above. C_{ant} values in the Pan-Antarctic were estimated from the averages of the four cold shelf regions above (equal to C_{ant} in Sum). The CO₂ uptake in Pan-Antarctic was estimated from the sum of all CO₂ uptake fluxes in all shelves (both cold and non-cold shelves in Figure 3), details in Table S5 of the Supporting Information S1.

$$G(t) = \sqrt{\frac{\Gamma^3}{4\pi\Delta^2t^3}} \exp\left(\frac{-\Gamma(t-\Gamma)^2}{4\Delta^2t}\right) \quad (9)$$

where the concentration of a passive tracer at a location, r , and time, t , $c(r, t)$, is related to the surface water history $c_0(t)$. $G(r, t)$ is the TTD of the tracer. The input function of the tracers, $c_0(t)$, is determined using the atmospheric history of the tracers and their salinity and temperature dependent solubility. Γ is the mean age and Δ is the width of the TTD (Waugh et al., 2004). The considered transit time distribution assumes that advection (0) and mixing (1) processes are globally of the same order of magnitude ($\Delta/\Gamma = 1$). The surface saturation of CFC-12 here was assumed to be 80% (Shao et al., 2013).

$$C_{\text{ant_ttt}}(t) = \int_0^\infty C_{\text{ant},0}(t-t')G(t')dt' \quad (10)$$

where $C_{\text{ant},0}(t-t')$ is the surface time history of C_{ant} and $G(t)$ is the TTD, as determined from CFC-12. The surface time history of C_{ant} is estimated as the difference between modern and pre-industrial DIC concentrations, that is, $C_{\text{ant},0}(t) = C_{\text{eq}}(T, S, \text{TA}^0, p\text{CO}_2(t)) - C_{\text{eq}}(T, S, \text{TA}^0, p\text{CO}_2 = 280 \text{ ppm})$, where C_{eq} is the DIC, T is temperature, S is salinity, TA^0 is the preformed alkalinity and $p\text{CO}_2(t)$ is the partial pressure of atmospheric CO₂ at time t (Waugh et al., 2006).

2.3. Calculation of Carbon Export Flux

To obtain a conservative estimate of C_{ant} and DIC export from the shelf region (e.g., Prydz Bay), we assumed that Dense Shelf Water (DSW) derived from the shelf region (Prydz Bay and Cape Darnley) contributed to about 6%–13% ($0.52 \pm 0.26 \text{ Sv}$) of the AABW flux (Ohshima et al., 2013). The downward transport of C_{ant} is associated with the formation of DSW, the subsequent offshore outflow, and the intrusion of the modified upwelling deep waters (mCDW) (Shadwick et al., 2014). Therefore, the gross export flux was calculated based on the mean C_{ant} value of the offshore export flux along the layer characterized by neutral density (γ_n) > 28.27 kg m⁻³ and $\theta < -1.85^\circ\text{C}$ (Equation 11); the net C_{ant} export flux was calculated based on the difference in mean C_{ant} values between the descending and upwelling water masses (Equation 12, Table S3 in Supporting Information S1). For other DSW ventilation rates we used $3.40 \pm 0.60 \text{ Sv}$ in the Weddell Sea (Akhoudas et al., 2021), $0.98 \pm 0.93 \text{ Sv}$ in the Ross Sea (Whitworth III & Orsi, 2006), $0.30 \pm 0.28 \text{ Sv}$ in the Adélie and George V Land coasts (Williams et al., 2010). The total ventilation rate is $5.20 \pm 0.32 \text{ Sv}$ for the four cold shelves, and $5.40 \pm 1.70 \text{ Sv}$ for the entire Pan-Antarctic region (Orsi et al., 2002). We took the average value of C_{ant} concentrations (Table 1) for different water masses during 1974–2018 to present a mean state (similar to climatological state) flux of the period. The uncertainty for export flux is given in Text S4 of the Supporting Information S1.

$$\Delta C_{\text{ant}}^{\text{gross-export}} = C_{\text{DSW_ant}} * V^{\text{DSW}} * \Delta t * \rho^{\text{DSW}} * m_c \quad (11)$$

$$\Delta C_{\text{ant}}^{\text{net-export}} = C_{\text{DSW_ant}} * V^{\text{DSW}} * \Delta t * \rho^{\text{DSW}} * m_c - C_{\text{mCDW_ant}} * V^{\text{mCDW}} * \Delta t * \rho^{\text{mCDW}} * m_c \quad (12)$$

where C_{ant} flux is in a unit of Tg C year⁻¹, V^{DSW} is the annual DSW ventilation rate (Sv; $10^6 \text{ m}^3 \text{ s}^{-1}$), Δt is the time period, ρ^{DSW} is the mean density of DSW, and m_c is the molar mass of carbon (g C mol^{-1}).

2.4. Quantification of Long-Term AABW pH Trends

pH deseasonalization: To avoid the seasonal biases in pH, which can be large in the polar ocean (Qi et al., 2022), we adopted a deseasonalization calculation as suggested by Takahashi et al. (2009). The difference between a monthly mean and the annual mean represents the correction to be applied to deseasonalize the monthly mean. Assuming that the seasonal variability and hence the deseasonalization corrections remain unchanged over time (Takahashi et al., 2009), we obtained the deseasonalized pH and its interannual rate of change.

Pressure normalization: pH observations were spatially unevenly distributed sampled, which could lead to a bias due to the over-weighted influence of high-dense data points concentrated in a particular area of the pressure layer. It might also affect our judgment of the long-term trend of pH in the AABW (Figure S5 in Supporting Information S1), according to the definition of AABW water masses ($\gamma_n > 28.27 \text{ kg m}^{-3}$, depth $> 2,000 \text{ m}$ in Table S3 of the Supporting Information S1) in this study. Therefore, we normalized the depth of the AABW to a mean depth (3,484 m), $\text{pH}_{\text{pressure}} = f(\text{DIC}, \text{TA}, S, T, 3,484, \text{Si}, \text{PO}_4^{3-})$.

2.5. Driver of the Long-Term pH Trend in AABW

We used a first order Taylor-series deconvolution (Kwiatkowski & Orr, 2018; Ouyang et al., 2020; Sarmiento & Gruber, 2006) to decompose the drivers (including temperature (T), salinity (S), DIC, TA) of pH temporal changes, as shown in Equation 13:

$$d\text{pH} = \frac{\partial\text{pH}}{\partial T} \times dT + \frac{\partial\text{pH}}{\partial\text{DIC}} \times d\text{DIC} + \frac{\partial\text{pH}}{\partial\text{TA}} \times d\text{TA} + \frac{\partial\text{pH}}{\partial S} \times dS + \frac{\partial\text{pH}}{\partial\text{fw}} \times d\text{fw} \quad (13)$$

$$\frac{\partial\text{pH}}{\partial\text{fw}} \times d\text{fw} = \left(\frac{s\text{DIC}}{S_0} \frac{\partial\text{pH}}{\partial\text{DIC}} + \frac{s\text{TA}}{S_0} \frac{\partial\text{pH}}{\partial\text{TA}} + \frac{S}{S_0} \frac{\partial\text{pH}}{\partial S} \right) \times dS \quad (14)$$

$$d\text{pH} = \frac{\partial\text{pH}}{\partial T} \times dT + \frac{\partial\text{pH}}{\partial\text{DIC}} \times \frac{S}{S_0} \times d(sC_{\text{ant}} + sC_{\text{nat}}) + \frac{\partial\text{pH}}{\partial\text{TA}} \times \frac{S}{S_0} \times ds\text{TA} + \left(\frac{s\text{DIC}}{S_0} \frac{\partial\text{pH}}{\partial\text{DIC}} + \frac{s\text{TA}}{S_0} \frac{\partial\text{pH}}{\partial\text{TA}} + \frac{S}{S_0} \frac{\partial\text{pH}}{\partial S} \right) \times dS \quad (15)$$

$$\frac{d\Delta^{\text{LT}}\text{pH}}{dt} = \frac{\partial\text{pH}}{\partial T} \times \frac{\Delta^{\text{LT}}T}{dt} + \frac{\partial\text{pH}}{\partial\text{DIC}} \times \frac{S}{S_0} \times \frac{\Delta^{\text{LT}}(sC_{\text{ant}} + sC_{\text{nat}})}{dt} + \frac{\partial\text{pH}}{\partial\text{TA}} \times \frac{S}{S_0} \times \frac{\Delta^{\text{LT}}\text{TA}}{dt} + \left(\frac{s\text{DIC}}{S_0} \frac{\partial\text{pH}}{\partial\text{DIC}} + \frac{s\text{TA}}{S_0} \frac{\partial\text{pH}}{\partial\text{TA}} + \frac{S}{S_0} \frac{\partial\text{pH}}{\partial S} \right) \times \frac{\Delta^{\text{LT}}S}{dt} \quad (16)$$

The partial derivatives of pH with respect to the respective drivers, $\partial\text{pH}/\partial T$, $\partial\text{pH}/\partial S$, $\partial\text{pH}/\partial\text{TA}$, and $\partial\text{pH}/\partial\text{DIC}$, were calculated by allowing a small change (1%) in temperature, salinity, TA and DIC respectively, while keeping all the other parameters constant (Table S4 in Supporting Information S1) (Orr et al., 2015). In addition, since freshwater fluxes (term fw) will induce changes in salinity, DIC and TA, it is useful to separate the freshwater effects from other biogeochemical processes, as in Equation 14 (Ouyang et al., 2020). We further separated DIC into C_{ant} and natural DIC (C_{nat}), to determine the anthropogenic impact and natural impacts on pH, C_{nat} values were determined as the difference between DIC and C_{ant} in Equation 15. $s\text{DIC}$, $s\text{TA}$, sC_{ant} , and sC_{nat} are the salinity normalized deviations from the annual means of DIC, TA, C_{ant} , and C_{nat} ($sX = X \cdot S_0 / S$). Both have been calculated taking into account the effects of meltwater (Friis et al., 2003; Ouyang et al., 2020). S and S_0 correspond to the observed and reference salinity (the average values of S in the AABW during 1974–2018), and the ratio between them approximates 1. The long-term changes in pH, $d\Delta^{\text{LT}}\text{pH}/dt$ were then separated into thermal and non-thermal components in Equation 16. According to Equation 16, the long-term trend of pH can be attributed to three drivers, temperature, DIC, and salinity. The results of Equation 16 and its components are listed in Table 2.

To estimate the acidification of the AABW caused by anthropogenic CO_2 from pre-industrial times to the present (year 2018), we used CO2SYS to simulate this process. Here, we defined “ pH_{pre} ” as the pH in the pre-industrial period and “pH” as the observed pH. Since CO_2 intrusion does not affect TA, and we assumed that TA, temperature, and salinity were constant over time. We calculated the changes in pH ($\Delta\text{pH}_{C_{\text{ant}}}$) by removing C_{ant} (based on TrOCA method) from DIC and then applying the CO2SYS calculation, $\Delta\text{pH}_{C_{\text{ant}}} = \text{pH} - \text{pH}_{\text{pre}} = f(\text{TA}, \text{DIC},$

Table 2
Estimated Contributions to the Long-Term pH Trends in AABW of Pan-Antarctic From 1974 to 2018

	Driver	Driver rate of change (yr ⁻¹)	Changes in drivers (1974–2018)	Contribution to the long-term trends pH (units yr ⁻¹)
Thermal component	ΔT	$0.001 \pm 0.001^\circ\text{C}$	$0.04 \pm 0.05^\circ\text{C}$	-0.00001 ± 0.00002
Non-thermal Component	ΔsDIC	$0.15 \pm 0.04 \mu\text{mol kg}^{-1}\ast$	$6.73 \pm 1.59 \mu\text{mol kg}^{-1}$	-0.0005 ± 0.0001
	$\Delta\text{sDIC}_{\text{C}_{\text{ant}}}$ ^a	$0.14 \pm 0.03 \mu\text{mol kg}^{-1}\ast\ast$	$6.09 \pm 1.20 \mu\text{mol kg}^{-1}$	-0.0004 ± 0.0001
	$\Delta\text{sDIC}_{\text{C}_{\text{nat}}}$ ^a	$0.01 \pm 0.05 \mu\text{mol kg}^{-1}$	$0.64 \pm 1.99 \mu\text{mol kg}^{-1}$	-0.00004 ± 0.00014
	ΔsTA	$-0.05 \pm 0.03 \mu\text{mol kg}^{-1}$	$-2.10 \pm 1.36 \mu\text{mol kg}^{-1}$	-0.0001 ± 0.0001
	$\Delta\text{S}(\text{freshwater})$	$-0.0003 \pm 0.0001 \text{ ppt}$	$-0.013 \pm 0.003 \text{ ppt}^b$	0.000002 ± 0.000001
Sum			-0.03 ± 0.01	-0.0006 ± 0.0002
Observed			-0.03 ± 0.00	-0.0006 ± 0.0001
C_{ant} pre-industrial-2018			-0.04 ± 0.01	

Note. The thermal and non-thermal components were separated by normalizing the pH to $S = 34.66$ (the mean salinity value of the AABW in four regions). Rates (\pm standard error of slope) were estimated by linear regression using annual means. Asterisks indicate the levels of significance of the trends ($\ast\ast P < 0.01$, $\ast P < 0.05$).

^aThe $\Delta\text{DIC}_{\text{C}_{\text{ant}}}$ and $\Delta\text{DIC}_{\text{C}_{\text{nat}}}$ indicate the changes in DIC due to anthropogenic CO_2 (TrOCA-based) and natural CO_2 . ^bParts per thousand (ppt) measures the salinity of seawater.

$S, T) - f(\text{TA}_{\text{pre}}, \text{DIC} - C_{\text{ant}}, S_{\text{pre}}, T_{\text{pre}})$. We found that pH has decreased by -0.04 ± 0.01 (Table 2) due to the additional anthropogenic CO_2 since pre-industrial time.

3. Results and Discussion

3.1. AABW Delivers Anthropogenic Carbon Into the Deep Ocean

Three approaches estimating C_{ant} concentrations agree with each other regarding the patterns and trends (Table 1; Figures S6 and S7, Text S5 in Supporting Information S1), all suggesting a hotspot of C_{ant} accumulation from the shelf through the slope to the deep ocean (Figure 1). In addition, these values are also comparable to previous studies reporting C_{ant} for different water masses at similar sites around Antarctica (Table 1), for instance, C_{ant} of DSW in the Ross Sea ($20\text{--}30 \mu\text{mol kg}^{-1}$; Chen, 1994; Sandrini et al., 2007) and the Adélie Land ($44 \mu\text{mol kg}^{-1}$, Shadwick et al., 2014), and C_{ant} of mCDW ($10\text{--}20 \mu\text{mol kg}^{-1}$; Lo Monaco, Goyet, et al., 2005; Lo Monaco, Metzl, et al., 2005; Pardo et al., 2014) and AABW in the Southern Ocean ($12\text{--}20 \mu\text{mol kg}^{-1}$; Lo Monaco, Goyet, et al., 2005; Lo Monaco, Metzl, et al., 2005; Pardo et al., 2014), respectively. It is worth noting that estimations from TrOCA and ΔC^\ast appear to exhibit greater coherence compared to those from TrOCA and TTD due to the same basic assumption in the backward calculation (Figures S6 and S7 in Supporting Information S1). However, the TTD approach is subject to a series of assumptions (particularly the “constant-with-time disequilibrium of carbon between atmosphere and surface ocean”; see Section 2.2) that are challenging to satisfy across diverse regions of the Southern Ocean, leading to inconsistent estimates of C_{ant} between TrOCA and TTD in the Weddell Sea and Prydz Bay.

Our results show that C_{ant} decreases with depth from the slope to the deep basin. The overall pattern of C_{ant} distribution in four cold-shelf regions (Figure 1) appeared to be consistent with CFC-12 (Figure S8 in Supporting Information S1). Maximum C_{ant} concentrations in the shelf waters were found in the DSW, while minimum C_{ant} values were found in the mCDW (Figure 1). We found that the shelf waters in cold shelf regions had higher C_{ant} concentrations ($40\text{--}50 \mu\text{mol kg}^{-1}$) than those in the adjacent basin (Figure 1), although they were still lower than those in other open oceans with a high C_{ant} of $60\text{--}70 \mu\text{mol kg}^{-1}$ (Huang et al., 2022; Sabine et al., 2004). More importantly, we also found hotspots of high C_{ant} in the AABW flowing along the Antarctic slope, below the cores of slightly contaminated (i.e., with low C_{ant} at present days) CDW in the adjacent basin.

This further reveals the evolution of carbon transport originating from the formation of DSW, which is triggered by sea-ice production and brine rejection, and subsequently sinks with CO_2 from the atmosphere (Figure 2a). A strong carbon transport efficiency could accelerate the transfer of newly absorbed C_{ant} from the shelf to the

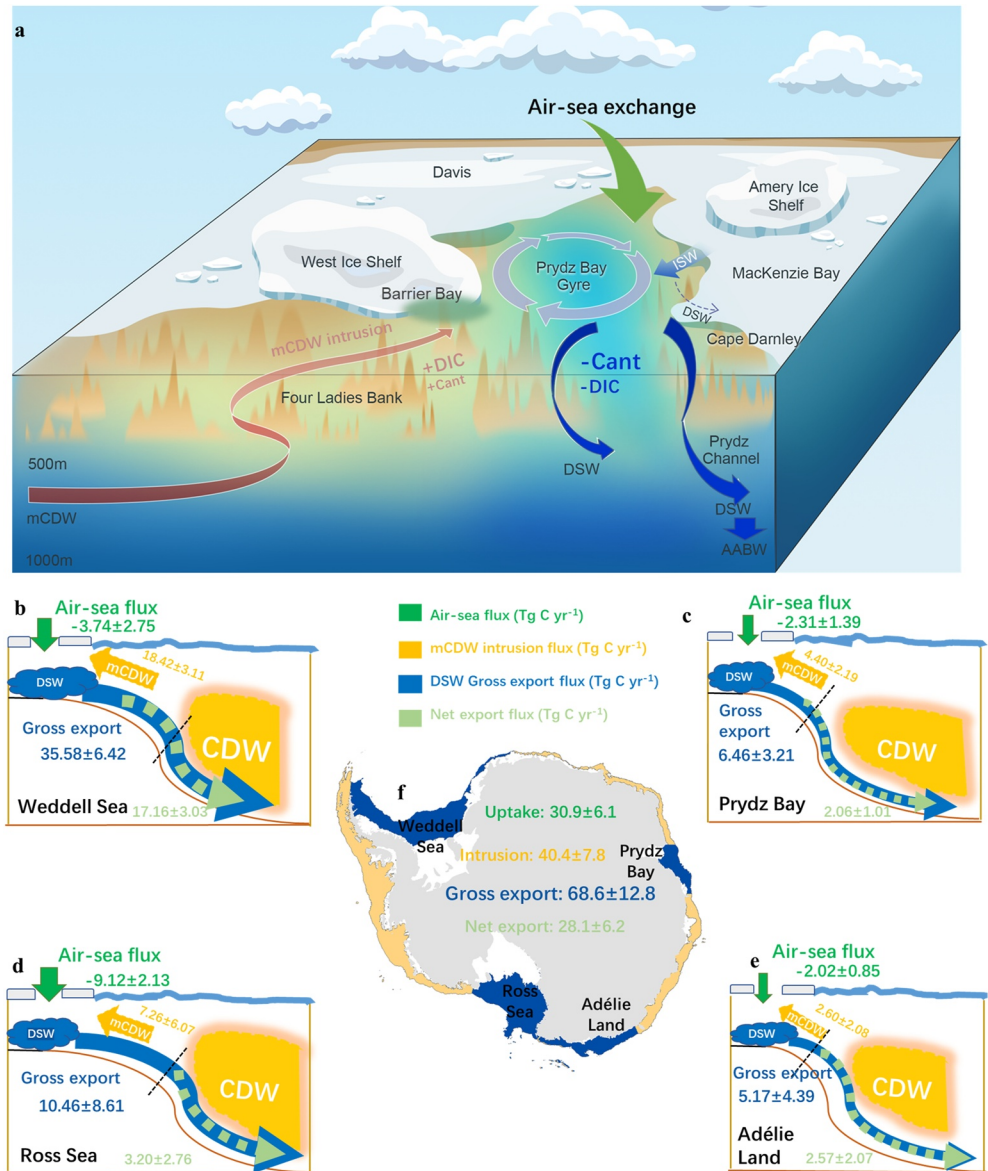


Figure 2. An overview of anthropogenic carbon (C_{ant}) export fluxes in the Pan-Antarctic. (a) Schematic view of carbon transport in the Prydz Bay. (a) The carbon (C_{ant} and DIC) transport during AABW formation involves mCDW intrusion shelf and DSW formation. The DSW (marked with blue) with high DIC and C_{ant} concentrations is transported downwards along the continental slope, where it continuously entrains CDW (marked with red) with high DIC and low C_{ant} and then subducts to form the AABW. (b–e) C_{ant} export fluxes in four cold AABW formation areas, including (b) Weddell Sea, (c) Prydz Bay, (d) Ross Sea, (e) Adélie Land. Carbon can be exported both within the DSW (values in blue) and mCDW (values in orange) across the shelf break (black dotted line). The air-sea CO_2 fluxes are in green and the net carbon export fluxes are in light green (negative values indicate carbon sink). All C_{ant} fluxes are presented as positive values, arrows indicate the direction of flux. The range of numbers in the figures is derived from the uncertainty of C_{ant} estimated using two methods and water mass ventilation rates (Equations 11 and 12 in Section 2). By extrapolating the average value of C_{ant} from the four cold shelves to the entire Pan-Antarctica, we obtained the C_{ant} export fluxes of the Pan-Antarctica (values in center figure (f)).

deep basin instead of accumulating in the shelf, resulting in a high C_{ant} concentration in the AABW during its formation (Figure 1). In the cold shelf regions, there are typically two pathways for the transport of DSW to the deep ocean. Taking Prydz Bay as an example (Figure 2a), the high CO_2 uptake (Figure 3; Table S6 in Supporting Information S1) observed in the Prydz Bay coincided with the high concentrations of C_{ant} in the underlying shelf waters (Figure 1 and Table 1). The primary DSW that sources from Cape Darnley flowed directly out along the western flank and through the Prydz Channel, then migrated northwest as gravity current to eventually joined the

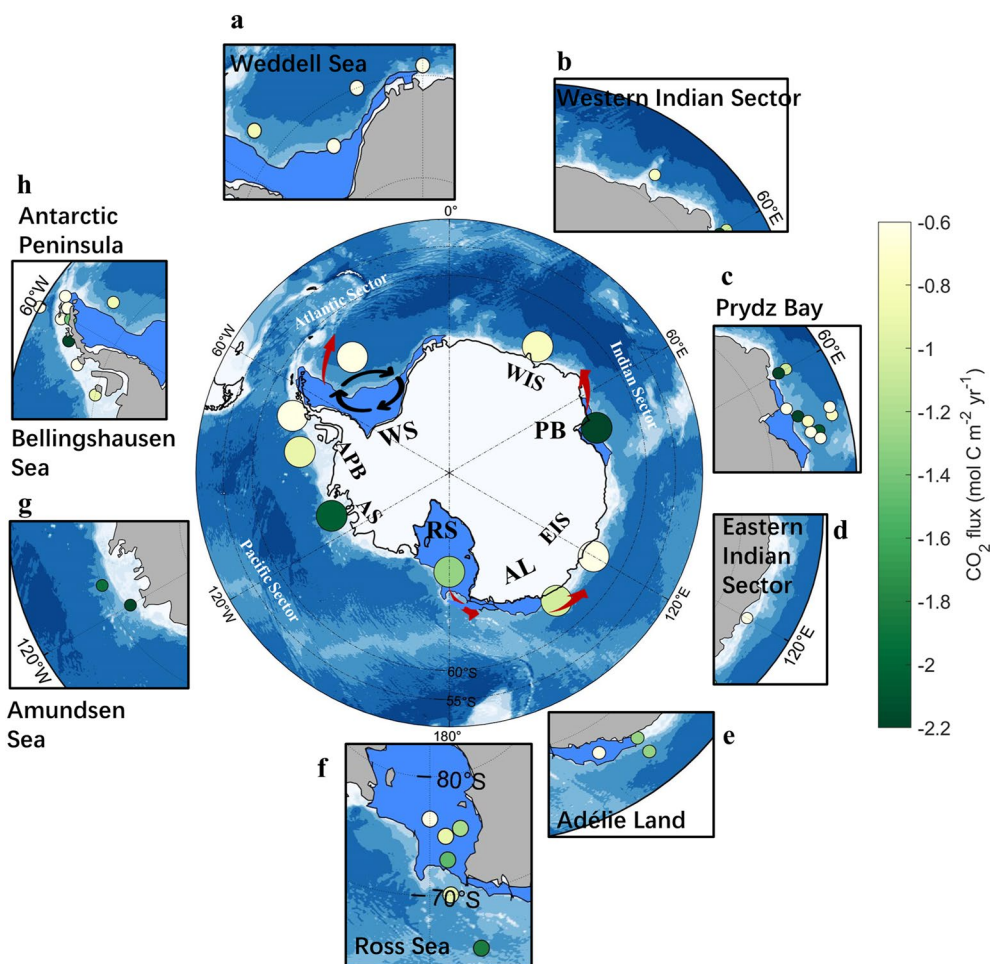


Figure 3. The updated annual air-sea CO_2 flux ($\text{mol C m}^{-2} \text{yr}^{-1}$) around the Pan-Antarctic. The updated annual air-sea CO_2 flux in the center shows the mean value of CO_2 flux from each sub-region. The separating sub-figures are the CO_2 flux calculated from the daily fluxes that have been reported previously (see details in Table S5 of the Supporting Information S1). The four cold shelves filled with sky blue are (a) Weddell Sea shelf region (WS), (c) Prydz Bay shelf region (PB), (e) Adélie Land shelf region (AL), (f) Ross Sea shelf region (RS). The non-cold shelf regions are (b) Western Indian Sector (WIS), (d) Eastern Indian Sector (EIS), (g) Amundsen Sea shelf region (AS), (h) Antarctic Peninsula and Bellingshausen Sea shelf region (APB). The thick red arrows indicate the direction of AABW from main sources to the Southern Ocean. Positive values indicate a carbon source, negative values indicate a carbon sink. Units of flux are in $\text{mol C m}^{-2} \text{yr}^{-1}$. Figures were made with Matlab version R2022a (The MathWorks Inc, 2022).

very saline DSW from Cape Darnley (Williams et al., 2016). Our observation also captured the downslope movement of DSW (high concentrations of C_{ant} and CFC-12) and its mixing with CDW (low concentrations of C_{ant} and CFC-12) over the shelf in the east Prydz Bay (Figure 1; Figure S8 in Supporting Information S1), which showed another pathway for the DSW (following the western flank of the trough/sill and meeting the eastern boundary of the Cape Darnley ice barrier) (Williams et al., 2016). Both pathways were the sources of the DSW, precursor water that contributes to the formation of AABW with high concentrations of C_{ant} and CFC-12 (Figure 2). Therefore, DSW was expected to remain in the upper layer long enough to reach CO_2 equilibrium with the atmosphere as much as possible, and then flow relatively quickly downwards and westwards to reach the deep Southern Ocean with higher C_{ant} concentrations (Roden et al., 2016).

3.2. A Greater Pan-Antarctic Export Flux Than Previously Thought

We then estimated the gross flux of C_{ant} for the four AABW formation regions, and then integrated them to obtain the C_{ant} gross flux (“gross” is defined as the total C_{ant} export flux via the subduction of the DSW to form the AABW, see Section 2 and Table 1), which is $57.7 \pm 12.0 \text{ Tg C yr}^{-1}$ based on C_{ant} in the DSW by TrOCA (Table 1)

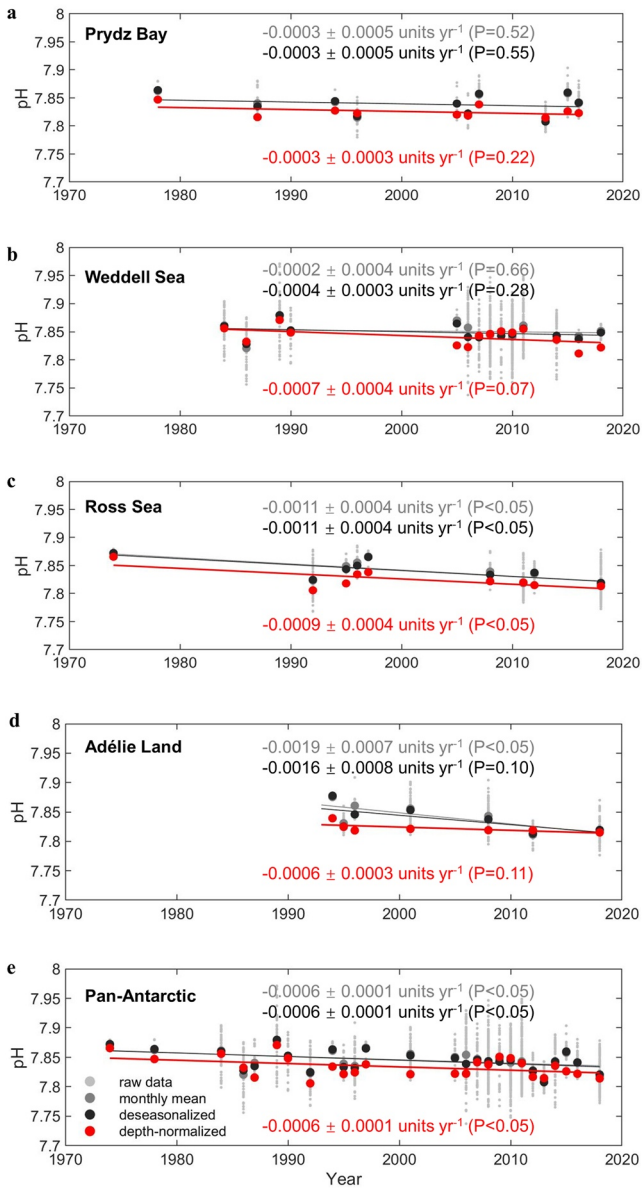


Figure 4. Long-term trends of pH in the deep Southern Ocean (AABW). The dark gray and the gray dots indicate the monthly mean of observed pH, and the raw observations in (a) Prydz Bay, (b) Weddell Sea, (c) Ross Sea, (d) Adélie Land, (e) Pan-Antarctic (the total of four cold shelf regions). The black and red dots in (a)–(e) indicate the deseasonalized monthly mean pH and the depth-normalized monthly mean pH after deseasonalization, respectively. The dark gray, black and red solid lines show linear regressions and the rates of change are shown in each panel, corresponding to the observed monthly mean, the deseasonalized monthly mean and the depth-normalized monthly mean, respectively. The pH values in (a)–(e) were obtained from the Global Data Analysis Project version 2022 database and CHINARE 31st.

according to Equation 11. We further upscaled this magnitude to the broader Pan-Antarctic cold shelf, including four AABW formation regions and polynyas (Kitade et al., 2014) by multiplying the average C_{ant} concentration from the four AABW formation regions by the total DSW ventilation rate in the Pan-Antarctic (5.40 ± 1.70 Sv) (Orsi et al., 2002). The broader Pan-Antarctic cold shelves have a gross C_{ant} export flux of 68.6 ± 12.8 Tg C yr⁻¹ (Figure 2f and Table 1), demonstrating that cold shelf regions dominate the carbon export from the shelf to the deep ocean in the Pan-Antarctica.

We also evaluated the net export flux for individual regions as this could determine the local carbon sink status. We obtained the net C_{ant} flux (“net” is defined as the residual C_{ant} export flux after deducting the supplied C_{ant} from the upwelling of mCDW; Equation 12, Table 1) for each AABW formation region (Figures 2b–2e and Table 1). Applying the same principle, the net C_{ant} flux was 25.0 ± 4.7 Tg C yr⁻¹ in the four cold shelves and 28.1 ± 6.2 Tg C yr⁻¹ when extrapolated to the broader Pan-Antarctic cold shelves. This mean value of Pan-Antarctic shelf C_{ant} export flux was comparable to the air-sea CO₂ uptake (-30.9 ± 6.1 Tg C yr⁻¹, Text S2 in Supporting Information S1, Figures 2 and 3, Table 1, and Table S5 in Supporting Information S1) of the Pan-Antarctica, implying that the downward export of carbon could subsequently sustain the surface air-sea CO₂ uptake.

3.3. Pan-Antarctic Carbon Transport Drives Strong Deep-Water Acidification

The export of CO₂-rich and low-pH seawaters through the formation of DSW and AABW would further induce declines in pH, which is referred to as ocean acidification (OA). The Ross Sea is found to exhibit the most rapid acidification (Figure 4c); however, this signal is primarily attributed to the single data point with a relatively higher pH value in 1974 during the period of 1974–1992, which may potentially lead to an overestimation of the acidification rate. We now investigate the long-term trend of pH (Figure 4) and the aragonite and calcite saturation state (Ω_{arag} and Ω_{calcite} , Figures S9 and S10 in Supporting Information S1) in the AABW ($\gamma_n > 28.27$ kg m⁻³).

Notably, from 1974 to 2018, the mean acidification rate of AABW in the Pan-Antarctic region is about -0.0006 ± 0.0001 yr⁻¹ in pH (Figure 4). This magnitude of acidification is less than that in the surface Southern Ocean, which ranged from -0.0011 to -0.0024 yr⁻¹ during 1969–2019 (Gregor & Gruber, 2021; Iida et al., 2021; Leseurre et al., 2022; Mazloff et al., 2023; Midorikawa et al., 2012), however, it is already significantly faster than that of the deep waters in the global open ocean (< -0.0002 yr⁻¹), such as the Hawaii Ocean Time-series (HOT) and the European Station for Time series in the Ocean at the Canary Island (ESTOC) (Chen et al., 2017; Dore et al., 2009). We suggest that this is linked to the rapid transport of C_{ant} from cold shelves to the deep ocean, because AABW contains C_{ant} from more recent years than the bottom waters at these other locations it is compared with. The more recent C_{ant} in the AABW (Figure 5) is presumably higher because the atmospheric CO₂ was higher.

To test this hypothesis, we quantified and decomposed the drivers of long-term OA into thermal (driven by temperature change, Figure S11 in Supporting Information S1) and non-thermal (driven by salinity, DIC, and TA changes, Figure 5; Figures S12 and S13 in Supporting Information S1) components (see Section 2, Table 2, and Table S6 in Supporting Information S1). As temperature changed negligibly (2%), the pH decrease was mainly driven by the non-thermal effect (98%, Table 2). The main driver of the contemporary pH decrease (1974–2018) was the increasing DIC (contributing 76%),

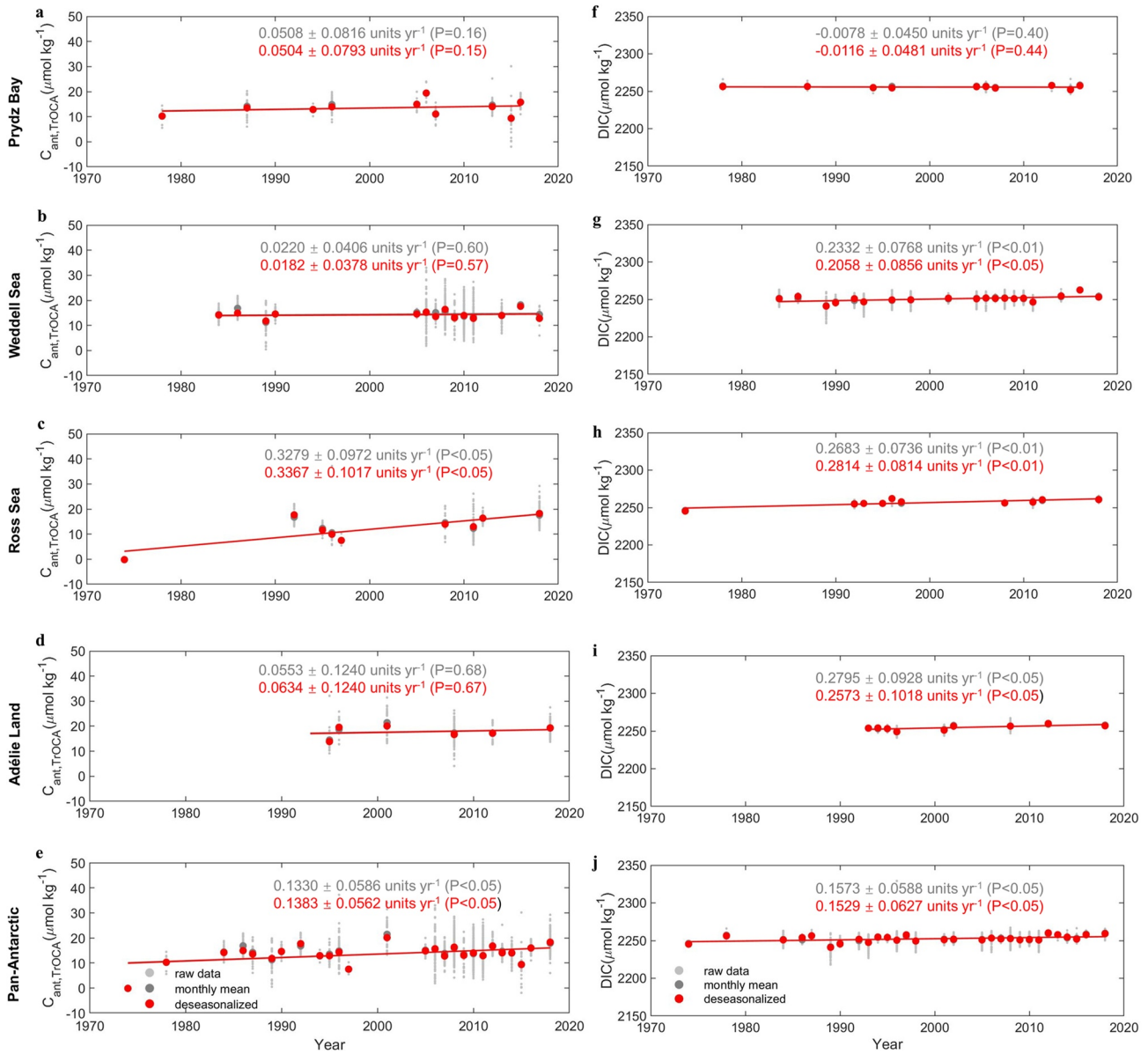


Figure 5. Long-term trends of C_{ant} and DIC in the deep Southern Ocean (AABW). The dark gray and the gray dots indicate the monthly mean of raw data C_{ant} and DIC, and the raw data in (a), (f) Prydz Bay, (b, g) Weddell Sea, (c, h) Ross Sea, (d, i) Adélie Land, (e, j) Pan-Antarctic (the total of four cold shelf regions). The red dots in (a)–(j) indicate the deseasonalized monthly mean C_{ant} and DIC. The dark gray and red solid lines show linear regressions and the rates of change are shown in each panel, corresponding to the raw data monthly mean, and the deseasonalized monthly mean. The DIC data in (f)–(j) were obtained from the Global Data Analysis Project version 2022 database and CHINARE 31st. C_{ant} was calculated by TrOCA method.

leading to a pH decrease of -0.0005 yr^{-1} in AABW, while TA contributed 23% with $-0.0001 \pm 0.0001 \text{ pH yr}^{-1}$. However, it should be noted that the trend in TA is statistically insignificant (Figure S13 in Supporting Information S1), and its role may be overstated. Due to the relatively small trend in pH, even a minor temporal change in TA ($-0.05 \text{ } \mu\text{mol kg}^{-1} \text{ yr}^{-1}$, equivalent to change of $2.2 \text{ } \mu\text{mol kg}^{-1}$ from 1974 to 2018) can make a significant contribution, although this change is just comparable to the uncertainty of TA measurement and therefore has negligible impact on CO2SYS and calculated pH. In addition, we observed an increase in temperature at a rate of $0.001 \pm 0.001 \text{ } ^\circ\text{C yr}^{-1}$ (Figure S11 in Supporting Information S1) in AABW in the Pan-Antarctic, and a faster decrease in salinity of $-0.0003 \pm 0.0001 \text{ yr}^{-1}$ (Table 2; Figure S12 in Supporting Information S1) in the cold shelf due to rapid downward transport of freshwater input from meltwater in these AABW formation regions (Williams et al., 2016). Although changes in temperature and salinity

contributed little to pH, they had a significant effect on the properties of AABW (Herraiz-Borreguero & Naveira Garabato, 2022), which has important implications for transport across the shelf (e.g., C_{ant}).

We further decomposed the changes in DIC (ΔsDIC) into a natural effect ($\Delta\text{sDIC}_{C_{\text{nat}}}$) and an anthropogenic effect ($\Delta\text{sDIC}_{C_{\text{ant}}}$). Our decomposition showed that, regarding the contribution of ΔsDIC term (76%) to a long-term decrease in pH, $\Delta\text{sDIC}_{C_{\text{ant}}}$ accounts for 69% and $\Delta\text{sDIC}_{C_{\text{nat}}}$ accounts for 7%, which could be due to anomalies in the biological pump, TA, zonal winds and ocean circulation in the cold Shelf (DeVries et al., 2017; Shi et al., 2021; Tagliabue & Arrigo, 2016). In addition, we estimated that an increase in C_{ant} has resulted in a pH change of -0.02 ± 0.01 (Table 2 and Figure 5) in the AABW from 1974 to 2018, and a pH change of -0.04 ± 0.01 (Figure S8 in Supporting Information S1 and $\Delta\text{pH}_{C_{\text{ant}}}$ in Section 2.5) from the pre-industrial period to 2018, which is close with previous studies (Jiang et al., 2019; Lauvset et al., 2020). It is worth noting that the change in pH in the AABW driven by C_{ant} from 1974 to 2018 accounts for almost $50\% \pm 30\%$ of the change since the pre-industrial period. Furthermore, the decrease in pH corresponds well with an increase in C_{ant} in waters deeper than 2,000 m (Figures 1, 4, and 5, and Figure S8 in Supporting Information S1), indicating that the rapid invasion and acceleration rates of C_{ant} (Figure 5) have been responsible for deep ocean acidification over the past four decades. The uptake and transport of C_{ant} is critical to the interpretation of the acidified AABW, which then drives acidification in the other ocean basins and would affect the organisms living in those waters, especially phytoplankton and invertebrates, and ultimately the marine ecosystem (Hancock et al., 2020).

4. Conclusions and Implications

Taken together, our work raises the possibility that the Antarctic continental shelf plays a larger role in the global ocean carbon cycle than previously thought, and the potential stress (acidification) on deep-sea ecology in the context of global change. Under the global warming scenario, warmer and faster CDW inflow (Shi et al., 2021) and increased freshwater input from the ice sheet could potentially result in less dense shelf water and reduced AABW formation, leading to a weaker downward carbon flux (Herraiz-Borreguero & Naveira Garabato, 2022; Nissen et al., 2022). On the other hand, the frequent climate anomalies could also lead to episodes of enhanced sea-ice formation that counteract the effects of ice sheet melting, leading to the rebound of the dense shelf water (Castagno et al., 2019) and the recovery of AABW formation (Silvano et al., 2020). These would add further complexity to the long-term variability of anthropogenic carbon export, and thus feed back to the carbon uptake capacity of the surface ocean. Therefore, in the face of such a complex and multi-factorial influenced dynamic process in shelf-slope systems, sustained observations and further investigations are needed.

Acknowledgments

This work was supported by the National Key Research and Development Program of China (2019YFE0114800), National Natural Science Foundation of China (42106222), Independent Research Projects of Southern Marine Science and Engineering Guangdong Laboratory (Zhuhai) (SML2021SP306), and Natural Science Foundation of Fujian Province, China (2020J05075). We are thankful to the numerous data contributors, scientists, technicians, and funding agencies responsible for the collection and production of GLODAP database. We are thankful to the crews of the Chinese National Arctic Research Expedition on board R/V *Xuelong*, as well as National Arctic and Antarctic Data Center from China. We thank Zhengbing Han and Jianming Pan, from the Second Institute of Oceanography, Ministry of Natural Resources, China, for providing the data of nutrients and the dissolved oxygen (DO). We also thank colleagues from GEOMAR, Zhiqiang Chen, Zhendong Hu, and Kaigui Fan for their assistance in data processing.

Conflict of Interest

The authors declare no conflicts of interest relevant to this study.

Data Availability Statement

Data—The DIC, TA, phosphate, silicate, nitrate, oxygen, temperature, salinity and CFC-12 data used to calculate anthropogenic CO_2 concentration and related variables were from the Global Ocean Data Analysis Project (GLODAP) version 2022 (Lauvset et al., 2022) and the 31st Chinese Antarctic Research Expedition (CHINARE) archived in the Mendeley Data repository (Chen, 2023). **Software**—data were analyzed with Matlab version R2022a (The MathWorks Inc, 2022), figures were made with Matlab version R2022a and Ocean Data View version 5.6.2 (Schlitzer, 2023).

References

- Akhoudas, C. H., Sallée, J.-B., Haumann, F. A., Meredith, M. P., Garabato, A. N., Reverdin, G., et al. (2021). Ventilation of the abyss in the Atlantic sector of the Southern Ocean. *Scientific Reports*, 11(1), 6760. <https://doi.org/10.1038/s41598-021-86043-2>
- Anderson, L. A., & Sarmiento, J. L. (1994). Redfield ratios of remineralization determined by nutrient data analysis. *Global Biogeochemical Cycles*, 8(1), 65–80. <https://doi.org/10.1029/93gb03318>
- Arrigo, K. R., van Dijken, G., & Long, M. (2008). Coastal Southern Ocean: A strong anthropogenic CO_2 sink. *Geophysical Research Letters*, 35(21), L21602. <https://doi.org/10.1029/2008gl035624>

- Bopp, L., Lévy, M., Resplandy, L., & Sallée, J. B. (2015). Pathways of anthropogenic carbon subduction in the global ocean. *Geophysical Research Letters*, 42(15), 6416–6423. <https://doi.org/10.1002/2015gl065073>
- Bourgeois, T., Orr, J. C., Resplandy, L., Terhaar, J., Ethé, C., Gehlen, M., & Bopp, L. (2016). Coastal-ocean uptake of anthropogenic carbon. *Biogeosciences*, 13(14), 4167–4185. <https://doi.org/10.5194/bg-13-4167-2016>
- Broecker, W. S. (1974). “NO”, a conservative water-mass tracer. *Earth and Planetary Science Letters*, 23(1), 100–107. [https://doi.org/10.1016/0012-821x\(74\)90036-3](https://doi.org/10.1016/0012-821x(74)90036-3)
- Castagno, P., Capozzi, V., DiTullio, G., Falco, P., Fusco, G., Rintoul, S. R., et al. (2019). Rebound of shelf water salinity in the Ross Sea. *Nature Communications*, 10(1), 5441. <https://doi.org/10.1038/s41467-019-13083-8>
- Chen, C. (1994). Some indications of excess CO₂ penetration near Cape Adare off the Ross Sea. *Oceanographic Literature Review*, 6(42), 441.
- Chen, C.-T. A., Lui, H.-K., Hsieh, C.-H., Yanagi, T., Kosugi, N., Ishii, M., & Gong, G.-C. (2017). Deep oceans may acidify faster than anticipated due to global warming. *Nature Climate Change*, 7(12), 890–894. <https://doi.org/10.1038/s41558-017-0003-y>
- Chen, L. (2023). Concentrations of anthropogenic carbon dioxide in the Prydz Bay in 2015 (version 2) [Dataset]. Mendeley Data. <https://data.mendeley.com/datasets/kk7c4f6473/2>
- de Lavergne, C., Palter, J. B., Galbraith, E. D., Bernardello, R., & Marinov, I. (2014). Cessation of deep convection in the open Southern Ocean under anthropogenic climate change. *Nature Climate Change*, 4(4), 278–282. <https://doi.org/10.1038/nclimate2132>
- DeVries, T. (2014). The oceanic anthropogenic CO₂ sink: Storage, air-sea fluxes, and transports over the industrial era. *Global Biogeochemical Cycles*, 28(7), 631–647. <https://doi.org/10.1002/2013gb004739>
- DeVries, T., Holzer, M., & Primeau, F. (2017). Recent increase in oceanic carbon uptake driven by weaker upper-ocean overturning. *Nature*, 542(7640), 215–218. <https://doi.org/10.1038/nature21068>
- Dickson, A., Chris, S., & Christian, J. R. (2007). *Guide to best practices for ocean CO₂ measurements*. (Vol. 3). North Pacific Marine Science Organization.
- Dickson, A. G. (1990). Standard potential of the reaction: AgCl(s)+1/2 H₂(g)=Ag(s)+HCl(aq), and the standard acidity constant of the ion HSO₄⁻ in synthetic seawater from 273.15 to 318.15 K. *Journal of Chemical Thermodynamics*, 22(2), 113–127. [https://doi.org/10.1016/0021-9614\(90\)90074-z](https://doi.org/10.1016/0021-9614(90)90074-z)
- Dore, J. E., Lukas, R., Sadler, D. W., Church, M. J., & Karl, D. M. (2009). Physical and biogeochemical modulation of ocean acidification in the central North Pacific. *Proceedings of the National Academy of Sciences of the United States of America*, 106(30), 12235–12240. <https://doi.org/10.1073/pnas.0906044106>
- Du, J., Ye, Y., Zhang, X., Völker, C., & Tian, J. (2022). Southern control of interhemispheric synergy on glacial marine carbon sequestration. *Geophysical Research Letters*, 49(16), e2022GL099048. <https://doi.org/10.1029/2022gl099048>
- Foster, T. D., & Carmack, E. C. (1976). Frontal zone mixing and Antarctic bottom water formation in the southern Weddell Sea. *Deep-Sea Research*, 23(4), 301–317. [https://doi.org/10.1016/0011-7471\(76\)90872-x](https://doi.org/10.1016/0011-7471(76)90872-x)
- Friis, K., Körtzinger, A., & Wallace, D. W. R. (2003). The salinity normalization of marine inorganic carbon chemistry data. *Geophysical Research Letters*, 30(2), 1085. <https://doi.org/10.1029/2002gl015898>
- Gao, H., Cai, W.-J., Jin, M., Dong, C., & Timmerman, A. H. V. (2022). Ocean ventilation controls the contrasting anthropogenic CO₂ uptake rates between the western and eastern South Atlantic Ocean basins. *Global Biogeochemical Cycles*, 36(6), e2021GB007265. <https://doi.org/10.1029/2021gb007265>
- Gregor, L., & Gruber, N. (2021). OceanSODA-ETHZ: A global gridded data set of the surface ocean carbonate system for seasonal to decadal studies of ocean acidification. *Earth System Science Data*, 13(2), 777–808. <https://doi.org/10.5194/essd-13-777-2021>
- Gruber, N. (1998). Anthropogenic CO₂ in the Atlantic Ocean. *Global Biogeochemical Cycles*, 12(1), 165–191. <https://doi.org/10.1029/97gb03658>
- Gruber, N., Clement, D., Carter, B. R., Feely, R. A., van Heuven, S., Hoppema, M., et al. (2019). The oceanic sink for anthropogenic CO₂ from 1994 to 2007. *Science*, 363(6432), 1193–1199. <https://doi.org/10.1126/science.aau5153>
- Gruber, N., & Sarmiento, J. L. (1997). Global patterns of marine nitrogen fixation and denitrification. *Global Biogeochemical Cycles*, 11(2), 235–266. <https://doi.org/10.1029/97gb00077>
- Gruber, N., Sarmiento, J. L., & Stocker, T. F. (1996). An improved method for detecting anthropogenic CO₂ in the oceans. *Global Biogeochemical Cycles*, 10(4), 809–837. <https://doi.org/10.1029/96gb01608>
- Hancock, A. M., King, C. K., Stark, J. S., McMinn, A., & Davidson, A. T. (2020). Effects of ocean acidification on Antarctic marine organisms: A meta-analysis. *Ecology and Evolution*, 10(10), 4495–4514. <https://doi.org/10.1002/ece3.6205>
- Herraiz-Borreguero, L., & Naveira Garabato, A. C. (2022). Poleward shift of Circumpolar Deep Water threatens the East Antarctic Ice Sheet. *Nature Climate Change*, 12(8), 728–734. <https://doi.org/10.1038/s41558-022-01424-3>
- Heuzé, C. (2021). Antarctic bottom water and North Atlantic deep water in CMIP6 models. *Ocean Science*, 17(1), 59–90. <https://doi.org/10.5194/os-17-59-2021>
- Huang, P., Wang, W., Chen, F., Cai, M., Ke, H., Liu, M., et al. (2022). Spatial and temporal trends of anthropogenic carbon storage in typical marginal seas along the Asia continent in the northern hemisphere. *Science of the Total Environment*, 823, 153580. <https://doi.org/10.1016/j.scitotenv.2022.153580>
- Iida, Y., Takatani, Y., Kojima, A., & Ishii, M. (2021). Global trends of ocean CO₂ sink and ocean acidification: An observation-based reconstruction of surface ocean inorganic carbon variables. *Journal of Oceanography*, 77(2), 323–358. <https://doi.org/10.1007/s10872-020-00571-5>
- Ito, T., Woloszyn, M., & Mazloff, M. (2010). Anthropogenic carbon dioxide transport in the Southern Ocean driven by Ekman flow. *Nature*, 463(7277), 80–83. <https://doi.org/10.1038/nature08687>
- Jiang, L.-Q., Carter, B. R., Feely, R. A., Lauvset, S. K., & Olsen, A. (2019). Surface ocean pH and buffer capacity: Past, present and future. *Scientific Reports*, 9(1), 18624. <https://doi.org/10.1038/s41598-019-55039-4>
- Khatiwal, S., Primeau, F., & Hall, T. (2009). Reconstruction of the history of anthropogenic CO₂ concentrations in the ocean. *Nature*, 462(7271), 346–349. <https://doi.org/10.1038/nature08526>
- Kitade, Y., Shimada, K., Tamura, T., Williams, G., Aoki, S., Fukamachi, Y., et al. (2014). Antarctic bottom water production from the Vincennes Bay Polynya, East Antarctica. *Geophysical Research Letters*, 41(10), 3528–3534. <https://doi.org/10.1002/2014gl059971>
- Kwiatkowski, L., & Orr, J. C. (2018). Diverging seasonal extremes for ocean acidification during the twenty-first century. *Nature Climate Change*, 8(2), 141–145. <https://doi.org/10.1038/s41558-017-0054-0>
- Lauvset, S. K., Carter, B. R., Pérez, F. F., Jiang, L.-Q., Feely, R. A., Velo, A., & Olsen, A. (2020). Processes driving global interior ocean pH distribution. *Global Biogeochemical Cycles*, 34(1), e2019GB006229. <https://doi.org/10.1029/2019gb006229>
- Lauvset, S. K., Lange, N., Tanhua, T., Bittig, H. C., Olsen, A., Kozyr, A., et al. (2022). GLODAPv2.2022: The latest version of the global interior ocean biogeochemical data product [Dataset]. *Earth System Science Data*, 14(12), 5543–5572. <https://doi.org/10.5194/essd-14-5543-2022>
- Lee, K., Kim, T.-W., Byrne, R. H., Millero, F. J., Feely, R. A., & Liu, Y. M. (2010). The universal ratio of boron to chlorinity for the North Pacific and North Atlantic oceans. *Geochimica et Cosmochimica Acta*, 74(6), 1801–1811. <https://doi.org/10.1016/j.gca.2009.12.027>

- Lee, S., Hwang, J., Ducklow, H. W., Hahm, D., Kim, D., et al. (2017). Evidence of minimal carbon sequestration in the productive Amundsen Sea polynya. *Geophysical Research Letters*, *44*(15), 7892–7899. <https://doi.org/10.1002/2017gl074646>
- Leseurre, C., Lo Monaco, C., Reverdin, G., Metzl, N., Fin, J., Mignon, C., & Benito, L. (2022). Summer trends and drivers of sea surface $f\text{CO}_2$ and pH changes observed in the southern Indian Ocean over the last two decades (1998–2019). *Biogeosciences*, *19*(10), 2599–2625. <https://doi.org/10.5194/bg-19-2599-2022>
- Liu, J., Wang, Y., & Chen, L. (2023). Carbon dioxide, hydrographic and chemical data collected from the profile discrete samples during the R/V Xuelong CHINARE2015 cruise (EXPOCODE 76XL20150203) in the Indian Ocean, Southern Ocean, Prydz Bay from 2015-02-03 to 2015-03-02 (NCEI Accession 0283240). [indicate subset used] [Dataset]. NOAA National Centers for Environmental Information. <https://doi.org/10.25921/0y42-ax52>
- Lo Monaco, C., Goyet, C., Metzl, N., Poisson, A., & Touratier, F. (2005). Distribution and inventory of anthropogenic CO_2 in the Southern Ocean: Comparison of three data-based methods. *Journal of Geophysical Research*, *110*(C9), C09S02. <https://doi.org/10.1029/2004jc002571>
- Lo Monaco, C., Metzl, N., Poisson, A., Brunet, C., & Schauer, B. (2005). Anthropogenic CO_2 in the Southern Ocean: Distribution and inventory at the Indian-Atlantic boundary (World Ocean Circulation Experiment line 16). *Journal of Geophysical Research*, *110*(C6), C06010. <https://doi.org/10.1029/2004jc002643>
- Lueker, T. J., Dickson, A. G., & Keeling, C. D. (2000). Ocean $p\text{CO}_2$ calculated from dissolved inorganic carbon, alkalinity, and equations for K1 and K2: Validation based on laboratory measurements of CO_2 in gas and seawater at equilibrium. *Marine Chemistry*, *70*(1), 105–119. [https://doi.org/10.1016/s0304-4203\(00\)00022-0](https://doi.org/10.1016/s0304-4203(00)00022-0)
- Mahieu, L., Lo Monaco, C., Metzl, N., Fin, J., & Mignon, C. (2020). Variability and stability of anthropogenic CO_2 in Antarctic bottom waters observed in the Indian sector of the Southern Ocean, 1978–2018. *Ocean Science*, *16*(6), 1559–1576. <https://doi.org/10.5194/os-16-1559-2020>
- Marinov, I., Gnanadesikan, A., Toggweiler, J. R., & Sarmiento, J. (2006). The Southern Ocean biogeochemical divide. *Nature*, *441*(7096), 964–967. <https://doi.org/10.1038/nature04883>
- Mazloff, M. R., Verdy, A., Gille, S. T., Johnson, K. S., Cornuelle, B. D., & Sarmiento, J. (2023). Southern Ocean acidification revealed by biogeochemical-Argo floats. *Journal of Geophysical Research: Oceans*, *128*(5), e2022JC019530. <https://doi.org/10.1029/2022jc019530>
- Midorikawa, T., Inoue, H. Y., Ishii, M., Sasano, D., Kosugi, N., Hashida, G., et al. (2012). Decreasing pH trend estimated from 35-year time series of carbonate parameters in the Pacific sector of the Southern Ocean in summer. *Deep Sea Research Part I: Oceanographic Research Papers*, *61*, 131–139. <https://doi.org/10.1016/j.dsr.2011.12.003>
- Mucci, A. (1983). The solubility of calcite and aragonite in seawater at various salinities, temperatures, and one atmosphere total pressure. *American Journal of Science*, *283*(7), 780–799. <https://doi.org/10.2475/ajs.283.7.780>
- Nissen, C., Timmermann, R., Hoppema, M., Gürses, Ö., & Hauck, J. (2022). Abruptly attenuated carbon sequestration with Weddell Sea dense waters by 2100. *Nature Communications*, *13*(1), 3402. <https://doi.org/10.1038/s41467-022-30671-3>
- Ohshima, K. I., Fukamachi, Y., Williams, G. D., Nishii, S., Roquet, F., Kitade, Y., et al. (2013). Antarctic bottom water production by intense sea-ice formation in the Cape Darnley polynya. *Nature Geoscience*, *6*(3), 235–240. <https://doi.org/10.1038/ngeo1738>
- Orr, J. C., Epitalon, J. M., & Gattuso, J. P. (2015). Comparison of ten packages that compute ocean carbonate chemistry. *Biogeosciences*, *12*(5), 1483–1510. <https://doi.org/10.5194/bg-12-1483-2015>
- Orsi, A. H., Smethie, W. M., Jr., & Bullister, J. L. (2002). On the total input of Antarctic waters to the deep ocean: A preliminary estimate from chlorofluorocarbon measurements. *Journal of Geophysical Research*, *107*(C8), 31–1–31–14. <https://doi.org/10.1029/2001jc000976>
- Ouyang, Z., Qi, D., Chen, L., Takahashi, T., Zhong, W., DeGrandpre, M. D., et al. (2020). Sea-ice loss amplifies summertime decadal CO_2 increase in the western Arctic Ocean. *Nature Climate Change*, *10*(7), 678–684. <https://doi.org/10.1038/s41558-020-0784-2>
- Pardo, P. C., Pérez, F. F., Khatiwala, S., & Ríos, A. F. (2014). Anthropogenic CO_2 estimates in the Southern Ocean: Storage partitioning in the different water masses. *Progress in Oceanography*, *120*, 230–242. <https://doi.org/10.1016/j.pocean.2013.09.005>
- Petty, A. A., Feltham, D. L., & Holland, P. R. (2013). Impact of atmospheric forcing on Antarctic continental shelf water masses. *Journal of Physical Oceanography*, *43*(5), 920–940. <https://doi.org/10.1175/jpo-d-12-0172.1>
- Poisson, A., & Chen, C.-T. A. (1987). Why is there little anthropogenic CO_2 in the Antarctic bottom water? *Deep Sea Research Part A: Oceanographic Research Papers*, *34*(7), 1255–1275. [https://doi.org/10.1016/0198-0149\(87\)90075-6](https://doi.org/10.1016/0198-0149(87)90075-6)
- Qi, D., Ouyang, Z., Chen, L., Wu, Y., Lei, R., Chen, B., et al. (2022). Climate change drives rapid decadal acidification in the Arctic Ocean from 1994 to 2020. *Science*, *377*(6614), 1544–1550. <https://doi.org/10.1126/science.abo0383>
- Rae, J. W. B., Burke, A., Robinson, L. F., Adkins, J. F., Chen, T., Cole, C., et al. (2018). CO_2 storage and release in the deep Southern Ocean on millennial to centennial timescales. *Nature*, *562*(7728), 569–573. <https://doi.org/10.1038/s41586-018-0614-0>
- Ríos, A. F., Velo, A., Pardo, P. C., Hoppema, M., & Pérez, F. F. (2012). An update of anthropogenic CO_2 storage rates in the western South Atlantic basin and the role of Antarctic Bottom Water. *Journal of Marine Systems*, *94*, 197–203. <https://doi.org/10.1016/j.jmarsys.2011.11.023>
- Roden, N. P., Tilbrook, B., Trull, T. W., Virtue, P., & Williams, G. D. (2016). Carbon cycling dynamics in the seasonal sea-ice zone of East Antarctica. *Journal of Geophysical Research: Oceans*, *121*(12), 8749–8769. <https://doi.org/10.1002/2016jc012008>
- Sabine, C., Feely, R., Key, R., Bullister, J., Millero, F. J., Lee, K., et al. (2002). Distribution of anthropogenic CO_2 in the Pacific Ocean. *Global Biogeochemical Cycles*, *16*(4), 30–1–30–17. <https://doi.org/10.1029/2001gb001639>
- Sabine, C. L., Feely, R. A., Gruber, N., Key, R. M., Lee, K., Bullister, J. L., et al. (2004). The oceanic sink for anthropogenic CO_2 . *Science*, *305*(5682), 367–371. <https://doi.org/10.1126/science.1097403>
- Sallée, J.-B., Matear, R. J., Rintoul, S. R., & Lenton, A. (2012). Localized subduction of anthropogenic carbon dioxide in the Southern Hemisphere oceans. *Nature Geoscience*, *5*(8), 579–584. <https://doi.org/10.1038/ngeo1523>
- Sandrini, S., Ait-Ameur, N., Rivaro, P., Massolo, S., Touratier, F., Tositti, L., & Goyet, C. (2007). Anthropogenic carbon distribution in the Ross Sea, Antarctica. *Antarctic Science*, *19*(3), 395–407. <https://doi.org/10.1017/s0954102007000405>
- Sarmiento, J. L., & Gruber, N. (2006). *Ocean biogeochemical dynamics*. Princeton University Press.
- Sarmiento, J. L., Orr, J. C., & Siegenthaler, U. (1992). A perturbation simulation of CO_2 uptake in an ocean general circulation model. *Journal of Geophysical Research*, *97*(C3), 3621–3645. <https://doi.org/10.1029/91jc02849>
- Schlitzer, R. (2023). Ocean data view (version 5.6.2) [Software]. <https://odv.awi.de>
- Shadwick, E. H., De Meo, O. A., Schroeter, S., Arroyo, M. C., Martinson, D. G., & Ducklow, H. (2021). Sea ice suppression of CO_2 outgassing in the West Antarctic Peninsula: Implications for the evolving Southern Ocean carbon sink. *Geophysical Research Letters*, *48*(11), e2020GL091835. <https://doi.org/10.1029/2020gl091835>
- Shadwick, E. H., Tilbrook, B., & Williams, G. D. (2014). Carbonate chemistry in the Mertz Polynya (East Antarctica): Biological and physical modification of dense water outflows and the export of anthropogenic CO_2 . *Journal of Geophysical Research: Oceans*, *119*(1), 1–14. <https://doi.org/10.1002/2013jc009286>
- Shao, A. E., Mecking, S., Thompson, L., & Sonnerup, R. E. (2013). Mixed layer saturations of CFC-11, CFC-12, and SF6 in a global isopycnal model. *Journal of Geophysical Research: Oceans*, *118*(10), 4978–4988. <https://doi.org/10.1002/jgrc.20370>

- Shi, J.-R., Talley, L. D., Xie, S.-P., Peng, Q., & Liu, W. (2021). Ocean warming and accelerating Southern Ocean zonal flow. *Nature Climate Change*, 11(12), 1090–1097. <https://doi.org/10.1038/s41558-021-01212-5>
- Silvano, A., Foppert, A., Rintoul, S. R., Holland, P. R., Tamura, T., Kimura, N., et al. (2020). Recent recovery of Antarctic bottom water formation in the Ross Sea driven by climate anomalies. *Nature Geoscience*, 13(12), 780–786. <https://doi.org/10.1038/s41561-020-00655-3>
- Solodoch, A., Stewart, A. L., Hogg, A. M., Morrison, A. K., Kiss, A. E., Thompson, A. F., et al. (2022). How does Antarctic bottom water cross the Southern Ocean? *Geophysical Research Letters*, 49(7), e2021GL097211. <https://doi.org/10.1029/2021gl097211>
- Tagliabue, A., & Arrigo, K. R. (2016). Decadal trends in air-sea CO₂ exchange in the Ross Sea (Antarctica). *Geophysical Research Letters*, 43(10), 5271–5278. <https://doi.org/10.1002/2016gl069071>
- Takahashi, T., Sutherland, S. C., Wanninkhof, R., Sweeney, C., Feely, R. A., Chipman, D. W., et al. (2009). Climatological mean and decadal change in surface ocean pCO₂, and net sea–air CO₂ flux over the global oceans. *Deep Sea Research Part II: Topical Studies in Oceanography*, 56(8–10), 554–577. <https://doi.org/10.1016/j.dsr2.2008.12.009>
- The MathWorks Inc. (2022). MATLAB version: 9.13.0 (R2022b) [Software]. The MathWorks Inc. Retrieved from <https://www.mathworks.com>
- Touratier, F., Azouzi, L., & Goyet, C. (2007). CFC-11, ¹⁴C and ³H tracers as a means to assess anthropogenic CO₂ concentrations in the ocean. *Tellus B: Chemical and Physical Meteorology*, 59(2), 318–325. <https://doi.org/10.1111/j.1600-0889.2006.00247.x>
- Touratier, F., & Goyet, C. (2004a). Applying the new TrOCA approach to assess the distribution of anthropogenic CO₂ in the Atlantic Ocean. *Journal of Marine Systems*, 46(1–4), 181–197. <https://doi.org/10.1016/j.jmarsys.2003.11.020>
- Touratier, F., & Goyet, C. (2004b). Definition, properties, and Atlantic Ocean distribution of the new tracer TrOCA. *Journal of Marine Systems*, 46(1–4), 169–179. <https://doi.org/10.1016/j.jmarsys.2003.11.016>
- van Heuven, S., Pierrot, D., Rae, J. W. B., Lewis, E., & Pierrot, D. (2011). MATLAB program developed for CO₂ system calculations. (Version 1.0) [Software]. ORNL/CDIAC-105b. Carbon Dioxide Information Analysis Center, Oak Ridge National Laboratory, U.S. Department of Energy. https://doi.org/10.3334/CDIAC/otg.CO2SYS_MATLAB_v1.1
- van Heuven, S. M. A. C., Hoppema, M., Huhn, O., Slagter, H. A., & de Baar, H. J. W. (2011). Direct observation of increasing CO₂ in the Weddell Gyre along the Prime Meridian during 1973–2008. *Deep Sea Research Part II: Topical Studies in Oceanography*, 58(25–26), 2613–2635. <https://doi.org/10.1016/j.dsr2.2011.08.007>
- Waugh, D. W., Haine, T. W. N., & Hall, T. M. (2004). Transport times and anthropogenic carbon in the subpolar North Atlantic Ocean. *Deep Sea Research Part I: Oceanographic Research Papers*, 51(11), 1475–1491. <https://doi.org/10.1016/j.dsr.2004.06.011>
- Waugh, D. W., Hall, T. M., McNeil, B. I., Key, R., & Matear, R. J. (2006). Anthropogenic CO₂ in the oceans estimated using transit time distributions. *Tellus B: Chemical and Physical Meteorology*, 58(5), 376–389. <https://doi.org/10.3402/tellusb.v58i5.17030>
- Whitworth, T., III., & Orsi, A. H. (2006). Antarctic bottom water production and export by tides in the Ross Sea. *Geophysical Research Letters*, 33(12). <https://doi.org/10.1029/2006gl026357>
- Williams, G. D., Aoki, S., Jacobs, S. S., Rintoul, S. R., Tamura, T., & Bindoff, N. L. (2010). Antarctic bottom water from the Adélie and George V land coast, East Antarctica (140–149°E). *Journal of Geophysical Research*, 115(C4), L12609. <https://doi.org/10.1029/2009jc005812>
- Williams, G. D., Herraiz-Borreguero, L., Roquet, F., Tamura, T., Ohshima, K. I., Fukamachi, Y., et al. (2016). The suppression of Antarctic bottom water formation by melting ice shelves in Prydz Bay. *Nature Communications*, 7(1), 12577. <https://doi.org/10.1038/ncomms12577>

References From the Supporting Information

- Álvarez, M., Ríos, A. F., & Rosón, G. (2002). Spatio-temporal variability of air–sea fluxes of carbon dioxide and oxygen in the Bransfield and Gerlache Straits during Austral summer 1995–96. *Deep Sea Research Part II: Topical Studies in Oceanography*, 49(4–5), 643–662. [https://doi.org/10.1016/s0967-0645\(01\)00116-3](https://doi.org/10.1016/s0967-0645(01)00116-3)
- Arrigo, K. R., & Van Dijken, G. L. (2007). Interannual variation in air-sea CO₂ flux in the Ross Sea, Antarctica: A model analysis. *Journal of Geophysical Research*, 112(C3), C03020. <https://doi.org/10.1029/2006jc003492>
- Arroyo, M. C., Shadwick, E. H., & Tilbrook, B. (2019). Summer carbonate chemistry in the Dalton Polynya, East Antarctica. *Journal of Geophysical Research: Oceans*, 124(8), 5634–5653. <https://doi.org/10.1029/2018jc014882>
- Arroyo, M. C., Shadwick, E. H., Tilbrook, B., Rintoul, S. R., & Kushara, K. (2020). A continental shelf pump for CO₂ on the Adélie Land Coast, East Antarctica. *Journal of Geophysical Research: Oceans*, 125(10), e2020JC016302. <https://doi.org/10.1029/2020jc016302>
- Bates, N. R., Hansell, D. A., Carlson, C. A., & Gordon, L. I. (1998). Distribution of CO₂ species, estimates of net community production, and air-sea CO₂ exchange in the Ross Sea polynya. *Journal of Geophysical Research*, 103(C2), 2883–2896. <https://doi.org/10.1029/97jc02473>
- Brown, P. J., Jullion, L., Landschützer, P., Bakker, D. C. E., Naveira Garabato, A. C., Meredith, M. P., et al. (2015). Carbon dynamics of the Weddell Gyre, Southern Ocean. *Global Biogeochemical Cycles*, 29(3), 288–306. <https://doi.org/10.1002/2014gb005006>
- Caetano, L. S., Pollery, R. C. G., Kerr, R., Magrani, F., Ayres Neto, A., Vieira, R., & Marotta, H. (2020). High-resolution spatial distribution of pCO₂ in the coastal Southern Ocean in late spring. *Antarctic Science*, 32(6), 476–485. <https://doi.org/10.1017/s0954102020000334>
- Chen, B., Cai, W.-J., & Chen, L. (2015). The marine carbonate system of the Arctic Ocean: Assessment of internal consistency and sampling considerations, summer 2010. *Marine Chemistry*, 176, 174–188. <https://doi.org/10.1016/j.marchem.2015.09.007>
- Constable, A. J., Melbourne-Thomas, J., Corney, S. P., Arrigo, K. R., Barbraud, C., Barnes, D. K. A., et al. (2014). Climate change and Southern Ocean ecosystems I: How changes in physical habitats directly affect marine biota. *Global Change Biology*, 20(10), 3004–3025. <https://doi.org/10.1111/gcb.12623>
- Costa, R. R., Mendes, C. R. B., Tavano, V. M., Dotto, T. S., Kerr, R., Monteiro, T., et al. (2020). Dynamics of an intense diatom bloom in the Northern Antarctic Peninsula, February 2016. *Limnology & Oceanography*, 65(9), 2056–2075. <https://doi.org/10.1002/lno.11437>
- Dai, M., Su, J., Zhao, Y., Hofmann, E. E., Cao, Z., Cai, W. J., et al. (2022). Carbon fluxes in the coastal ocean: Synthesis, boundary processes and future trends. *Annual Review of Earth and Planetary Sciences*, 50(1), 593–626. <https://doi.org/10.1146/annurev-earth-032320-090746>
- DeJong, H. B., & Dunbar, R. B. (2017). Air-sea CO₂ exchange in the Ross Sea, Antarctica. *Journal of Geophysical Research: Oceans*, 122(10), 8167–8181. <https://doi.org/10.1002/2017jc012853>
- Gao, Z., Chen, L., & Gao, Y. (2008). Air-sea carbon fluxes and their controlling factors in the Prydz Bay in the Antarctic. *Acta Oceanologica Sinica*(3), 136–146.
- Gibson, J. A., & Trull, T. W. (1999). Annual cycle of fCO₂ under sea-ice and in open water in Prydz Bay, East Antarctica. *Marine Chemistry*, 66(3–4), 187–200. [https://doi.org/10.1016/s0304-4203\(99\)00040-7](https://doi.org/10.1016/s0304-4203(99)00040-7)
- Gray, A. R., Johnson, K. S., Bushinsky, S. M., Riser, S. C., Russell, J. L., Talley, L. D., et al. (2018). Autonomous biogeochemical floats detect significant carbon dioxide outgassing in the high-latitude Southern Ocean. *Geophysical Research Letters*, 45(17), 9049–9057. <https://doi.org/10.1029/2018gl078013>

- Hoppema, M., Fahrbach, E., Stoll, M. H., & de Baar, H. J. (1999). Annual uptake of atmospheric CO₂ by the Weddell Sea derived from a surface layer balance, including estimations of entrainment and new production. *Journal of Marine Systems*, 19(4), 219–233. [https://doi.org/10.1016/S0924-7963\(98\)00091-8](https://doi.org/10.1016/S0924-7963(98)00091-8)
- Hoppema, M., Stoll, M. H. C., & de Baar, H. J. W. (2000). CO₂ in the Weddell Gyre and Antarctic circumpolar current: Austral autumn and early winter. *Marine Chemistry*, 72(2), 203–220. [https://doi.org/10.1016/S0304-4203\(00\)00082-7](https://doi.org/10.1016/S0304-4203(00)00082-7)
- Ishii, M., Inoue, H. Y., & Matsueda, H. (2002). Net community production in the marginal ice zone and its importance for the variability of the oceanic pCO₂ in the Southern Ocean south of Australia. *Deep Sea Research Part II: Topical Studies in Oceanography*, 49(9), 1691–1706. [https://doi.org/10.1016/S0967-0645\(02\)00007-3](https://doi.org/10.1016/S0967-0645(02)00007-3)
- Ito, R. G., Tavano, V. M., Mendes, C. R. B., & Garcia, C. A. E. (2018). Sea-air CO₂ fluxes and pCO₂ variability in the Northern Antarctic Peninsula during three summer periods (2008–2010). *Deep Sea Research Part II: Topical Studies in Oceanography*, 149, 84–98. <https://doi.org/10.1016/j.dsr2.2017.09.004>
- Laruelle, G. G., Dürr, H., Lauerwald, R., Hartmann, J., Slomp, C. P., Goossens, N., & Regnier, P. A. G. (2013). Global multi-scale segmentation of continental and coastal waters from the watersheds to the continental margins. *Hydrology and Earth System Sciences*, 17(5), 2029–2051. <https://doi.org/10.5194/hess-17-2029-2013>
- Laruelle, G. G., Landschützer, P., Gruber, N., Tison, J.-L., Delille, B., & Regnier, P. (2017). Global high-resolution monthly pCO₂ climatology for the coastal ocean derived from neural network interpolation. *Biogeosciences*, 14(19), 4545–4561. <https://doi.org/10.5194/bg-14-4545-2017>
- Laruelle, G. G., Lauerwald, R., Pfeil, B., & Regnier, P. (2014). Regionalized global budget of the CO₂ exchange at the air-water interface in continental shelf seas. *Global Biogeochemical Cycles*, 28(11), 1199–1214. <https://doi.org/10.1002/2014gb004832>
- Legge, O. J., Bakker, D. C., Johnson, M. T., Meredith, M. P., Venables, H. J., Brown, P. J., & Lee, G. A. (2015). The seasonal cycle of ocean-atmosphere CO₂ flux in Ryder Bay, west Antarctic Peninsula. *Geophysical Research Letters*, 42(8), 2934–2942. <https://doi.org/10.1002/2015gl063796>
- Long, M. C., Stephens, B. B., McKain, K., Sweeney, C., Keeling, R. F., Kort, E. A., et al. (2021). Strong Southern Ocean carbon uptake evident in airborne observations. *Science*, 374(6572), 1275–1280. <https://doi.org/10.1126/science.aba4355>
- McNeil, B. I., Metzl, N., Key, R. M., Matear, R. J., & Corbiere, A. (2007). An empirical estimate of the Southern Ocean air-sea CO₂ flux. *Global Biogeochemical Cycles*, 21(3). <https://doi.org/10.1029/2007gb002991>
- Metzl, N., Brunet, C., Jabaud-Jan, A., Poisson, A., & Schauer, B. (2006). Summer and winter air-sea CO₂ fluxes in the Southern Ocean. *Deep Sea Research Part I: Oceanographic Research Papers*, 53(9), 1548–1563. <https://doi.org/10.1016/j.dsr.2006.07.006>
- Monteiro, T., Kerr, R., & Machado, E. D. C. (2020). Seasonal variability of net sea-air CO₂ fluxes in a coastal region of the northern Antarctic Peninsula. *Scientific Reports*, 10(1), 14875. <https://doi.org/10.1038/s41598-020-71814-0>
- Monteiro, T., Kerr, R., Orselli, I. B. M., & Lencina-Avila, J. M. (2020). Towards an intensified summer CO₂ sink behaviour in the Southern Ocean coastal regions. *Progress in Oceanography*, 183, 102267. <https://doi.org/10.1016/j.poccean.2020.102267>
- Mu, L., Stammerjohn, S. E., Lowry, K. E., & Yager, P. L. (2014). Spatial variability of surface pCO₂ and air-sea CO₂ flux in the Amundsen Sea Polynya, Antarctica. *Elementa: Science of the Anthropocene*, 3. <https://doi.org/10.12952/journal.elementa.000036>
- Murakami, K., Nomura, D., Hashida, G., Nakaoka, S.-I., Kitade, Y., Hirano, D., et al. (2020). Strong biological carbon uptake and carbonate chemistry associated with dense shelf water outflows in the Cape Darnley polynya, East Antarctica. *Marine Chemistry*, 225, 103842. <https://doi.org/10.1016/j.marchem.2020.103842>
- Ogundare, M. O., Fransson, A., Chierici, M., Joubert, W. R., & Roychoudhury, A. N. (2021). Variability of sea-air carbon dioxide flux in autumn across the Weddell Gyre and offshore Dronning Maud Land in the Southern Ocean. *Frontiers in Marine Science*, 7. <https://doi.org/10.3389/fmars.2020.614263>
- Pardo, P. C., Pérez, F. F., Velo, A., & Gilcoto, M. (2012). Water masses distribution in the Southern Ocean: Improvement of an extended OMP (eOMP) analysis. *Progress in Oceanography*, 103, 92–105. <https://doi.org/10.1016/j.poccean.2012.06.002>
- Pfeil, B., Olsen, A., Bakker, D. C. E., Hankin, S., Koyuk, H., Kozyr, A., et al. (2013). A uniform, quality controlled Surface Ocean CO₂ Atlas (SOCAT). *Earth System Science Data*, 5(1), 125–143. <https://doi.org/10.5194/essd-5-125-2013>
- Prend, C. J., Gray, A. R., Talley, L. D., Gille, S. T., Haumann, F. A., Johnson, K. S., et al. (2022). Indo-Pacific sector dominates Southern Ocean carbon outgassing. *Global Biogeochemical Cycles*, 36(7), e2021GB007226. <https://doi.org/10.1029/2021gb007226>
- Roden, N. P., Shadwick, E. H., Tilbrook, B., & Trull, T. W. (2013). Annual cycle of carbonate chemistry and decadal change in coastal Prydz Bay, East Antarctica. *Marine Chemistry*, 155, 135–147. <https://doi.org/10.1016/j.marchem.2013.06.006>
- Romera-Castillo, C., Álvarez, M., Pelegrí, J. L., Hansell, D. A., & Álvarez-Salgado, X. A. (2019). Net additions of recalcitrant dissolved organic carbon in the deep Atlantic Ocean. *Global Biogeochemical Cycles*, 33(9), 1162–1173. <https://doi.org/10.1029/2018gb006162>
- Roobaert, A., Laruelle, G. G., Landschützer, P., Gruber, N., Chou, L., & Regnier, P. (2019). The spatiotemporal dynamics of the sources and sinks of CO₂ in the global coastal ocean. *Global Biogeochemical Cycles*, 33(12), 1693–1714. <https://doi.org/10.1029/2019gb006239>
- Sabine, C., & Gruber, N. (2005). Response to Comment on “The ocean sink for anthropogenic CO₂”. *Science*, 308(5729), 1743. <https://doi.org/10.1126/science.1109949>
- Sabine, C. L., Key, R. M., Johnson, K. M., Millero, F. J., Poisson, A., Sarmiento, J. L., et al. (1999). Anthropogenic CO₂ inventory of the Indian Ocean. *Global Biogeochemical Cycles*, 13(1), 179–198. <https://doi.org/10.1029/1998gb900022>
- Shadwick, E., Rintoul, S., Tilbrook, B., Williams, G., Young, N., Fraser, A. D., et al. (2013). Glacier tongue calving reduced dense water formation and enhanced carbon uptake. *Geophysical Research Letters*, 40(5), 904–909. <https://doi.org/10.1002/grl.50178>
- Shetye, S., Jena, B., & Mohan, R. (2017). Dynamics of sea-ice biogeochemistry in the coastal Antarctica during transition from summer to winter. *Geoscience Frontiers*, 8(3), 507–516. <https://doi.org/10.1016/j.gsf.2016.05.002>
- Sweeney, C. (2003). The annual cycle of surface water CO₂ and O₂ in the Ross Sea: A model for gas exchange on the continental shelves of Antarctica. *Biogeochemistry of the Ross Sea*, 78, 295–312. <https://doi.org/10.1029/078ars19>
- Tortell, P. D., Long, M. C., Payne, C. D., Alderkamp, A.-C., Dutrieux, P., & Arrigo, K. R. (2012). Spatial distribution of pCO₂, ΔO₂/Ar and dimethylsulfide (DMS) in polynya waters and the sea ice zone of the Amundsen Sea, Antarctica. *Deep Sea Research Part II: Topical Studies in Oceanography*, 71, 77–93. <https://doi.org/10.1016/j.dsr2.2012.03.010>
- Tozawa, M., Nomura, D., Nakaoka, S. I., Kiuchi, M., Yamazaki, K., Hirano, D., et al. (2021). Seasonal variations and drivers of surface ocean pCO₂ in the seasonal ice zone of the eastern Indian Sector, Southern Ocean. *Journal of Geophysical Research: Oceans*, 127(1), e2021JC017953. <https://doi.org/10.1029/2021jc017953>
- Wang, Y., Qi, D., Wu, Y., Gao, Z., Sun, H., Lin, H., et al. (2020). Biological and physical controls of pCO₂ and air-sea CO₂ fluxes in the austral summer of 2015 in Prydz Bay, East Antarctica. *Marine Chemistry*, 228, 103897. <https://doi.org/10.1016/j.marchem.2020.103897>
- Wu, Y., Bakker, D. C. E., Achterberg, E. P., Silva, A. N., Pickup, D. D., Li, X., et al. (2022). Integrated analysis of carbon dioxide and oxygen concentrations as a quality control of ocean float data. *Communications Earth & Environment*, 3(1), 92. <https://doi.org/10.1038/s43247-022-00421-w>
- Xu, S., Park, K., Wang, Y., Chen, L., Qi, D., & Li, B. (2019). Variations in the summer oceanic pCO₂ and carbon sink in Prydz Bay using the self-organizing map analysis approach. *Biogeosciences*, 16(3), 797–810. <https://doi.org/10.5194/bg-16-797-2019>

Erratum

In the originally published version of this article, authors Chengyan Liu, Qinghua Yang, Yiming Lu, and Xiao Cheng were incorrectly affiliated to “Centre for Southern Hemisphere Oceans Research (CSHOR), CSIRO Oceans and Atmosphere, Hobart, TAS, Australia.” The correct affiliation is “Southern Marine Science and Engineering Guangdong Laboratory (Zhuhai), Zhuhai, China.” The error has been corrected, and this version may be considered the authoritative version of record.